Design of thermo-piezoelectric microstructured bending actuators via multi-field asymptotic homogenization

Design of thermo-piezoelectric microstructured bending actuators via multi-field asymptotic homogenization

Francesca Fantoni[1,*], Andrea Bacigalupo[2,*], Marco Paggi[2]

[1] DICATAM, Università degli Studi di Brescia, via Branze 43, 25123, Brescia, Italy

[2] IMT School for Advanced Studies Lucca, Piazza S.Francesco 19, 55100 Lucca, Italy

June 11, 2018

Abstract

The use of integrated MicroElectroMechanical systems (MEMS) is recently spread thanks to their improved sensitivity, accuracy and reliability. Accurate preliminary computations born from the need of high precision in the manufacturing process of such devices. Piezoelectric materials are broadly employed in this field as direct converters between mechanical and electrical signals and some of these piezoelectric materials show pyroelectric features, which involve thermo-electrical interactions. Pyroelectric bending actuators are analyzed in the present study in plane conditions. They consists of active PZT layers with in-plane polarization and a microstructured composite layer characterized by a periodic microstructure where PZT fibers with an out of plane polarization are immersed in a polymeric matrix. The constitutive law of the composite layer at the mesoscale has been determined by means of a multi-field asymptotic homogenization technique, recently developed for thermo-piezoelectric materials. Overall constitutive equations characterizing the behavior of the microstructured layer at the mesoscale have been derived and the closed form of the overall constitutive tensors has been provided for the equivalent first-order (Cauchy) homogenized continuum. Deflection of unimorph and bimorph bender actuators has been investigated in relation to their geometrical features, exploiting the out of plane piezoelectric properties of the composite layer, which modify the stiffness of the entire bender. An accurate description of benders behavior at the structural length scale is of fundamental importance in order to design devices with high performances. In this regard, the influence of the microstructure on the global response of the actuator is investigated in the present study in order to understand how the composite material can be tailored to meet specific design requirements.

1 Introduction

Piezoelecricity is the property of some crystalline materials to generate an electric field if mechanically deformed (direct effect). Such deformation of the crystalline structure, which becomes electrically polarized, is completely reversible. The inverse piezoelectric effect on the contrary consists of experiencing mechanical deformations in the presence of an electric field (Yang, 2004). By virtue of these two principles, piezoelectric materials can be used to create sensors (direct effect) and actuators (inverse effect). Since the beginning of the twentieth century, scientific research related to piezoelectric materials has grown steadily (Brand et al., 2015; Kim et al., 2011; Anton and Sodano, 2007), fueled by the interest to fulfill industry needs, involving numerous engineering sectors, from electronic components (transformers, frequency generators) to telecommunications, from the automotive field (injection systems, vibration control) to the biomedical field.
Some piezoelectric materials are also pyroelectric. Pyroelectricity involves thermo-electrical interactions, being the polarization of the crystalline material dependent in this case on temperature (Moulson and Herbert, 2003; Batra and Aggarwal, 2013). For pyroelectric materials the nature of thermal gradient modifies the direction of the pyroelectric current and as a result of this change in temperature, the material becomes polarized establishing an electrical potential.

*Corresponding authors: Tel:+39 0583 4326613,
E-mail addresses: francesca.fantoni@unibs.it; andrea.bacigalupo@imtlucca.it

Restricting the attention on actuators, the most common piezo/pyroelectric devices are of two types: multilayer (or stack) actuators and benders. Stack actuators are created by layering multiple piezoelectric elements, each enclosed between two electrodes, taking advantage of their combined expansion in order to produce movement and force. Bender actuators, on the other hand, refer to two basic models: unimorph and bimorph. Unimorph bender consists of a piezoelectric layer and a passive one. Bimorph bender is characterized by a central passive layer sandwiched between two piezoelectric laminae. Electrodes are applied on the upper and lower surfaces of each piezoelectric layer (Kang and Wang, 2010; Yan et al., 2011). For this type of actuator, deformations induced by the electric field lead to deflection of the device which act as a cantilever.

Piezo/pyroelectric actuators are used for example as signal sources, micro and nano-positioning systems (Okazaki, 1990), micro-mirrors (Cheng et al., 2001), micro-grippers (Wang et al., 1999), vibration damping (Hagood and von Flotow, 1991) and noise control devices. Piezoelectric laminae are often made of Lead Zirconate Titanate ($P_b(Zr_xTi_{1-x})O_3$), commonly called PZT, which manifests excellent piezoelectric properties, including rapid signal response, large electro-mechanical coupling factor, physical and chemical stability, low energy consumption, and miniaturization potential.

Miniaturized and integrated microelectromechanical systems (MEMS) actuators and sensors are increasingly developed thanks to the recent advances in microprocessing technologies (Saadon and Sidek, 2011; Gardner et al., 2001). This leads to high precision manufacturing needs, with a remarkable demand of preliminary computations (Heinonen et al., 2007) which, in many cases, become cumbersome and time consuming.

In this regard, homogenization methods can be conveniently exploited in order to describe the effects of the microstructure on the overall behavior of the material in a rigorous and synthetic way, avoiding the challenging need to perform a numerical computation of the whole heterogeneous medium. Homogenization techniques therefore reveal to be an useful and convenient method to take into account the microstructural heterogeneity, especially in the case of periodic composite media, such as the above-mentioned multi-layered actuators.

The overall static and dynamic properties of periodic composite materials can generally be determined by asymptotic homogenization methods (Bacigalupo et al., 2016a,b; Bakhvalov and Panasenko, 1984; Bensoussan et al., 1978), variational-asymptotic techniques (Bacigalupo et al., 2014; Bacigalupo, 2014; Peerlings and Fleck, 2004; Smyshlyaev and Cherednichenko, 2000), and computational homogenization techniques (Trovalusci et al., 2017; De Bellis and Bacigalupo, 2017; Bacigalupo et al., 2017; Addessi et al., 2016, 2013; Bacca et al., 2013a,b,c; Bigoni and Drugan, 2007; Forest and Sab, 1998; Forest and Trinh, 2011; Miehe et al., 1999; Kouznetsova et al., 2004). Examples of asymptotic homogenization methods applied to multi-field problems can be found in (Galka et al., 1996, 1992) for thermo-electro-elastic materials and in (Sixto-Camacho et al., 2013; Bravo-Castillero et al., 2009) for the case of thermo-magneto-electro-elastic materials. They exclusively address first-order continuum problems. In this framework authors have recently formulated an asymptotic homogenization procedure for periodic thermo-piezoelectric materials including the closed form of higher order problems and the averaged field equations of infinite order obtained by means of an asymptotic expansion of the macro fields (Fantoni et al., 2017).

The present study aims at providing a characterization of deflection of multi-layered bending actuators, in particular unimorh and bimorph benders. They are considered made of one or two active piezoelectric laminae and a composite layer characterized by a periodic microstructure, which replaces the usual passive layer. The multi-field asymptotic homogenization technique described in (Fantoni et al., 2017) for periodic thermo-piezoelectric materials, is here exploited to describe the constitutive law of the microstructured composite layer at the mesoscale. It has been here restricted to the case of first-order multi-field homogenization and applied with the aim of investigating the optimal design of pyroelectric bending actuators. The exact closed forms of the overall thermo-piezoelectric tensors of the composite layer are determined for plane stress and plane strain conditions, thus avoiding the need to model the whole microstructured heterogeneous stratum. Field equations for the homogenized first-order thermo-piezoelectric medium are derived, following the procedure developed in (Bacigalupo and Gambarotta, 2014; Smyshlyaev and Cherednichenko, 2000; Bakhvalov and Panasenko, 1984) for composite elastic media with periodic microstructure and particularized by (Fantoni et al., 2017) to the case of thermo-piezoelectric materials. Analyzed benders remain heterogeneous at the structural length scale, being composed by the piezolectric laminae and the homogenized composite layer.

The paper is organized as follows. *Section* 2 is a brief summary of the proposed approach and it is devoted to stress the role of the asymptotic homogenization procedure in the final characterization of bender

actuators. In *Section 3* the geometry of a generic periodic thermo-piezoelectric composite material is illustrated and the corresponding constitutive equations and balance relations are introduced. The developed multi-field asymptotic homogenization technique is described in *Section 4*, based on down-scaling relations correlating the microscopic fields to the macroscopic ones. Resolution of a series of recursive non homogeneous differential problems, known as cell problems, whose domain is the unit periodic cell, allows to derive perturbation functions. They take into account the effects of the microstructural heterogeneity on the micro-fields and on the coupling between them. In the same *Section*, the obtained closed form of the overall constitutive tensors is shown for the equivalent first-order (Cauchy) homogenized medium and average field equations of infinite order are determined for the case at hand. These results are used in *Section 5* to derive overall tensors of a composite thermo-piezoelectric material with periodic microstructure characterized by circular or square inclusions. Deflection of unimorph and bimorph bender actuators has been numerically investigated varying the geometric features of the benders, loaded by imposed electric potential and relative temperature gradients. Finally, conclusions are reported in *Section 6*.

2 Synopsis of the proposed approach

One considers a multi-layer thermo-piezoelectric actuator as the one depicted in figure 1. Some of these layers can be characterized by a periodic microstructure with periodic cells that are properly described at the microstructural level. In this scenario it is possible to identify different characteristic lengths: the structural one l_s, the mesoscopic one l_M, and the microscopic one l_m.

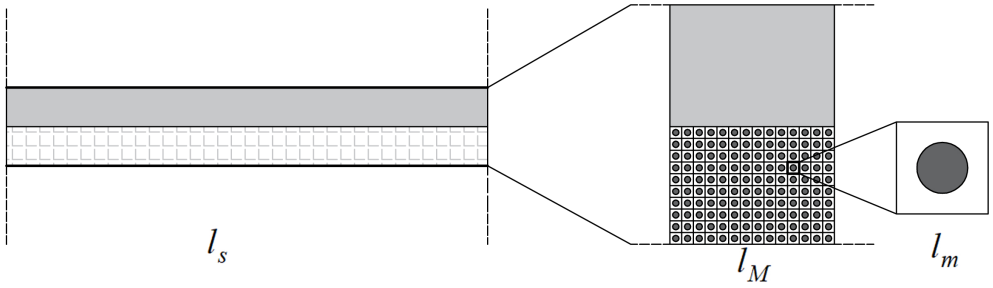

Figure 1: *Multi-scale description of a multi-layered thermo-piezoelectric actuator allows to identify three different characteristic length scales: the structural one l_s, the mesoscopic one l_M, and the microstructural one l_m at which the periodic cell is properly described.*

For the validity of the scales separability concept the size of the periodic cell is supposed to be much smaller than the overall height of the single layer and the ratio between different characteristic lengths has to be in a certain range such that $l_s >> l_M >> l_m$. A framework of the kind depicted in figure 1 is suitable for the formulation of a multi-scale asymptotic homogenization approach, which allows to move from the microscale to the structural length scale. The homogenization model here exploited is an asymptotic two-scales technique, whose goal is to move from the heterogeneous biphase medium with periodic microstructure, whose phases are described by a first order continuum model at the microstructural length scale l_m, to an equivalent homogeneous medium, described by a first order continuum model at the macro characteristic length scale l_M. Actuators considered in the present study are made by two (unimorph) or three (bimorph) layers and boundary conditions at the extrados and intrados of the devices do not allow to exploit a standard homogenization procedure to move from the mesoscale to the structural length scale. Therefore, at the macroscale the device is considered heterogeneous and made by two/three layers: one/two PZT layers and one composite layer whose overall constitutive properties are determined by means of the asymptotic homogenization technique introduced in (Fantoni et al., 2017) and here briefly described in *Sections* 3 and 4.

The aim of the present study is to investigate deflection of multi-layered bending actuators in relation to some geometrical parameters of the benders themselves, exploiting the pyroelectric and piezolelectric properties of the components in order to design high performance devices. After computing the overall tensors of the composite layer, the behavior of the bending actuators has been numerically investigated. To this purpose, numerical analyses have been performed by means of the finite element software FEAP, where an ad hoc

thermo-piezoelectric finite element has been implemented to solve the coupled thermo-electro-mechanical problem, exploiting the isoparametric concept to approximate the element geometry. Details regarding the formulation of such an element can be found in Appendix C of (Fantoni et al., 2017).
Alternative approaches to study the deflection of bender actuators can involve the derivation of analytical expressions for the bending curvature along benders length. For these techniques overall constitutive properties of benders'layers at the mesoscale constitute input parameters to solve the plane problem. There exists a vast literature devoted to the problem of determining the bending curvature of multi-layered piezoelectric actuators, each case characterized by different simplifying assumptions related to electro-mechanical material behavior, boundary conditions and external applied loads. From the work of Steel et al. (Steel et al., 1978), who derived tip deflection and stretching of unimorph piezoelectric benders as functions of applied electric voltage, to the profound analyses made by Smits et al. (Smits et al., 1991; Smits and Choi, 1991), who investigated the performance of bimorph piezoelectric benders under quasi-static conditions deriving the relations between applied mechanical and/or electrical loads and the response of the device in terms of bending angle, tip deflection, volume change and electrical charge. They considered a clamped cantilever beam condition on one side of the device and used a thermodynamical approach based on the computation of the electrical enthalpy of the system in order to compute the electrical and mechanical parameters of the piezoelectric device. Wang and Cross (Wang and Cross, 1999) derived analytical expression for the bending curvature for symmetric piezolectric bimorph benders under different loading conditions. De Lit et al. (De Lit et al., 2003) used a completely mechanical method to investigate the behavior of piezoelectric bending devices, treating these lasts as Euler beams for mechanical simplifications. They computed curvature, tip deflection, and tip angle based on equilibrium equations of forces and moments for a certain set of imposed boundary conditions, neglecting however the influence of the external loads onto the electrical parameters. More recently, Dunsch and Breguet (Dunsch and Breguet, 2007) investigated a static model for piezoelectric bender actuators subjected to a generic external load, assuming the validity of the Euler Bernoulli beam theory for the benders. They considered no slip between the different layers and computed quantities of interest under static equilibrium conditions for the beam.

3 Multiscale modeling of periodic thermo-piezoelectric composites

Under the validity of small strains assumption, the present multiscale description deals with heterogeneous composite media having a periodic microstructure, as the one shown in figure 2. Description of a linear thermo-piezoelectric Cauchy continuum presented in (Mindlin, 1974) is assumed in the present note. The medium is subject to three types of volume forces represented by body forces, free charge densities, and temperature changes.

Vector $\mathbf{x} = x_1\,\mathbf{e}_1 + x_2\,\mathbf{e}_2$ identifies the position of each material point in the continuum, with reference to the orthogonal coordinates system with origin at point O and base $\{\mathbf{e_1}, \mathbf{e}_2\}$ (see figure 2-(a)). Without losing generality, the notation has been restricted to the two dimensional case, for the sake of simplicity. Two orthogonal vectors $\mathbf{v}_1 = d_1\,\mathbf{e}_1 = \varepsilon\mathbf{e}_1$ and $\mathbf{v}_2 = d_2\,\mathbf{e}_2 = \delta\varepsilon\,\mathbf{e}_2$, with ε the characteristic size of the periodic cell $\mathcal{A} = [0, \varepsilon] \times [0, \delta\varepsilon]$, represent the periodicity vectors, as illustrated in figure 2-(b). The micro constitutive tensors, namely micro-elasticity tensor $\mathbb{C}^{(m,\varepsilon)}$, the micro-dielectric permittivity tensor (at constant strain) $\boldsymbol{\beta}^{(m,\varepsilon)}$, the micro-heat conduction tensor $\boldsymbol{K}^{(m,\varepsilon)}$, the micro piezoelectric stress/charge tensor $\boldsymbol{e}^{(m,\varepsilon)}$, the micro-thermal dilatation tensor $\boldsymbol{\alpha}^{(m,\varepsilon)}$, and the micro pyroelectric vector $\boldsymbol{\gamma}^{(m,\varepsilon)}$, obey the following properties by virtue of the $\mathcal{A}$ periodicity of the medium

$$\mathbb{C}^{(m,\varepsilon)}(\mathbf{x} + \mathbf{v}_i) = \mathbb{C}^{(m,\varepsilon)}(\mathbf{x}), \quad i = 1, 2, \quad \forall \mathbf{x} \in \mathcal{A}, \tag{1a}$$

$$\boldsymbol{\beta}^{(m,\varepsilon)}(\mathbf{x} + \mathbf{v}_i) = \boldsymbol{\beta}^{(m,\varepsilon)}(\mathbf{x}), \quad i = 1, 2, \quad \forall \mathbf{x} \in \mathcal{A}, \tag{1b}$$

$$\boldsymbol{K}^{(m,\varepsilon)}(\mathbf{x} + \mathbf{v}_i) = \boldsymbol{K}^{(m,\varepsilon)}(\mathbf{x}), \quad i = 1, 2, \quad \forall \mathbf{x} \in \mathcal{A}, \tag{1c}$$

$$\boldsymbol{e}^{(m,\varepsilon)}(\mathbf{x} + \mathbf{v}_i) = \boldsymbol{e}^{(m,\varepsilon)}(\mathbf{x}), \quad i = 1, 2, \quad \forall \mathbf{x} \in \mathcal{A}, \tag{1d}$$

$$\boldsymbol{\alpha}^{(m,\varepsilon)}(\mathbf{x} + \mathbf{v}_i) = \boldsymbol{\alpha}^{(m,\varepsilon)}(\mathbf{x}), \quad i = 1, 2, \quad \forall \mathbf{x} \in \mathcal{A}, \tag{1e}$$

$$\boldsymbol{\gamma}^{(m,\varepsilon)}(\mathbf{x} + \mathbf{v}_i) = \boldsymbol{\gamma}^{(m,\varepsilon)}(\mathbf{x}), \quad i = 1, 2, \quad \forall \mathbf{x} \in \mathcal{A}. \tag{1f}$$

$\mathcal{Q} = [0, 1] \times [0, \delta]$ is the non dimensional unit cell obtained from the periodic cell $\mathcal{A}$ rescaled by the mis-

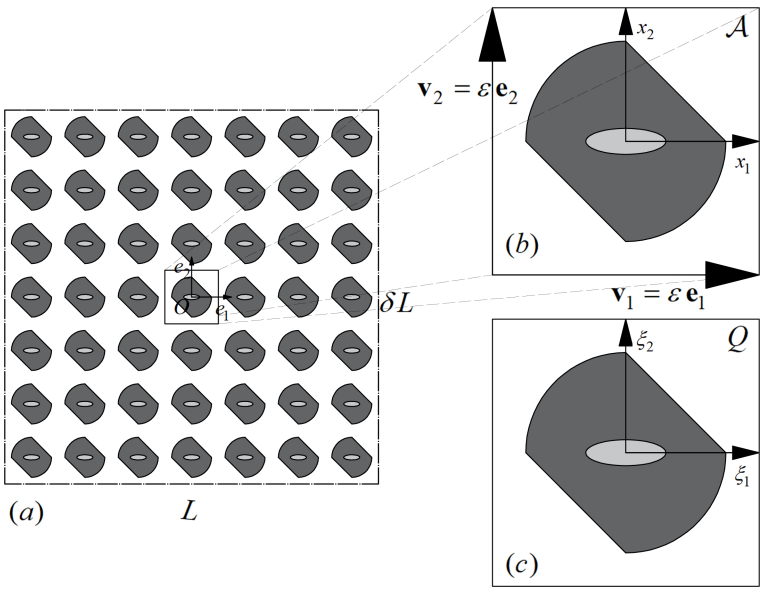

Figure 2: *(a) Heterogeneous composite medium with structural characteristic size L and periodic microstructure; (b)Periodic cell $\mathcal{A}$ with microstructural characteristic size ε and periodicity vectors $\mathbf{v}_1$ and $\mathbf{v}_2$; (c) Periodic unit cell $\mathcal{Q}$.*

crostructural length ε. Two separated scales, the macro and the micro ones, can be described respectively by two distinct variables: the macroscopic (or slow) one $\mathbf{x} \in \mathcal{A}$ and the microscopic (or fast) one $\boldsymbol{\xi} = \mathbf{x}/\varepsilon \in \mathcal{Q}$, as described in (Bacigalupo, 2014; Smyshlyaev, 2009; Peerlings and Fleck, 2004; Bakhvalov and Panasenko, 1984). Constitutive tensors (1a)-(1f) can consequently be defined over the unit cell $\mathcal{Q}$ as dependent only on the microscopic variable $\boldsymbol{\xi}$:

$$\begin{aligned}&\mathbb{C}^{(m,\varepsilon)}(\mathbf{x}) = \mathbb{C}^m(\boldsymbol{\xi} = \mathbf{x}/\varepsilon), \quad \boldsymbol{\beta}^{(m,\varepsilon)}(\mathbf{x}) = \boldsymbol{\beta}^m(\boldsymbol{\xi} = \mathbf{x}/\varepsilon), \quad \boldsymbol{K}^{(m,\varepsilon)}(\mathbf{x}) = \boldsymbol{K}^m(\boldsymbol{\xi} = \mathbf{x}/\varepsilon),\\ &\boldsymbol{e}^{(m,\varepsilon)}(\mathbf{x}) = \boldsymbol{e}^m(\boldsymbol{\xi} = \mathbf{x}/\varepsilon), \quad \boldsymbol{\alpha}^{(m,\varepsilon)}(\mathbf{x}) = \boldsymbol{\alpha}^m(\boldsymbol{\xi} = \mathbf{x}/\varepsilon), \quad \boldsymbol{\gamma}^{(m,\varepsilon)}(\mathbf{x}) = \boldsymbol{\gamma}^m(\boldsymbol{\xi} = \mathbf{x}/\varepsilon).\end{aligned} \tag{2}$$

The micro stress $\boldsymbol{\sigma}(\mathbf{x})$, the micro electric displacement $\mathbf{D}(\mathbf{x})$, and the micro heat flux $\mathbf{q}(\mathbf{x})$ are determined respectively by the following constitutive relations (Mindlin, 1974)

$$\boldsymbol{\sigma}(\mathbf{x}) = \mathbb{C}^{(m,\varepsilon)}(\mathbf{x})\,\boldsymbol{\varepsilon}(\mathbf{x}) + \boldsymbol{e}^{(m,\varepsilon)}(\mathbf{x})\,\nabla\phi(\mathbf{x}) - \boldsymbol{\alpha}^{(m,\varepsilon)}(\mathbf{x})\,\theta(\mathbf{x}), \tag{3a}$$

$$\mathbf{D}(\mathbf{x}) = \tilde{\boldsymbol{e}}^{(m,\varepsilon)}(\mathbf{x})\,\boldsymbol{\varepsilon}(\mathbf{x}) - \boldsymbol{\beta}^{(m,\varepsilon)}(\mathbf{x})\,\nabla\phi(\mathbf{x}) + \boldsymbol{\gamma}^{(m,\varepsilon)}(\mathbf{x})\,\theta(\mathbf{x}), \tag{3b}$$

$$\mathbf{q}(\mathbf{x}) = -\boldsymbol{K}^{(m,\varepsilon)}(\mathbf{x})\,\nabla\theta(\mathbf{x}), \tag{3c}$$

where $\tilde{e}^m_{ijk} = e^m_{jki}$ and the time derivative of $\mathbf{u}(\mathbf{x})$ and $\theta(\mathbf{x})$ has been neglected in equation (3c) in the hypothesis of quasi-static processes (Mindlin, 1974; Nowacki, 1986). The following local balance equations are satisfied respectively by the stress field $\boldsymbol{\sigma}(x)$, the electric displacement field $\mathbf{D}(\mathbf{x})$, and the heat flux $\mathbf{q}(x)$

$$\nabla\cdot\boldsymbol{\sigma}(\mathbf{x}) + \mathbf{b}(\mathbf{x}) = \mathbf{0}, \quad \nabla\cdot\mathbf{D}(\mathbf{x}) - \rho_e(\mathbf{x}) = 0, \quad \nabla\cdot\boldsymbol{q}(\mathbf{x}) + r(\mathbf{x}) = 0, \tag{4}$$

where volume forces are represented by body forces $\mathbf{b}(\mathbf{x})$, free charge densities $\rho_e(\mathbf{x})$, and heat sources $r(\mathbf{x})$, all dependent only on the slow variable $\mathbf{x}$. Volume forces are assumed to be $\mathcal{L}$-periodic, with vanishing mean values on $\mathcal{L}$, being $\mathcal{L} = [0, L] \times [0, \delta L]$. $\mathcal{L}$ can be contemplated as a true representative portion of the whole body, because, for the scales separation condition, the structural length L is much greater than the microstructural one ε ($L >> \varepsilon$).

Substituting constitutive equations (3a)-(3c) into balance equations (4), one obtains the following set of partial differential equations:

$$\nabla\cdot\left(\mathbb{C}^{(m,\varepsilon)}(\mathbf{x})\,\nabla\mathbf{u}(\mathbf{x})\right) + \nabla\cdot\left(\boldsymbol{e}^{(m,\varepsilon)}(\mathbf{x})\,\nabla\phi(\mathbf{x})\right) - \nabla\cdot\left(\boldsymbol{\alpha}^{(m,\varepsilon)}(\mathbf{x})\,\theta(\mathbf{x})\right) + \mathbf{b}(\mathbf{x}) = \mathbf{0}, \tag{5a}$$

$$\nabla\cdot\left(\tilde{\boldsymbol{e}}^{(m,\varepsilon)}(\mathbf{x})\,\nabla\mathbf{u}(\mathbf{x})\right) - \nabla\cdot\left(\boldsymbol{\beta}^{(m,\varepsilon)}(\mathbf{x})\,\nabla\phi(\mathbf{x})\right) + \nabla\cdot\left(\boldsymbol{\gamma}^{(m,\varepsilon)}(\mathbf{x})\,\theta(\mathbf{x})\right) - \rho_e(\mathbf{x}) = 0, \tag{5b}$$

$$\nabla \cdot \left(\boldsymbol{K}^{(m,\varepsilon)}(\mathbf{x}) \nabla\theta(\mathbf{x}) \right) + r(\mathbf{x}) = 0. \tag{5c}$$

Continuity conditions can be expressed in the following way for a perfectly bounded interface Σ:

$$[[\mathbf{u}(\mathbf{x})]]|_{\boldsymbol{x}\in\Sigma} = \mathbf{0}, \quad \left[\left[\left(\mathbb{C}^{(m,\varepsilon)}(\mathbf{x})\nabla\mathbf{u}(\mathbf{x}) + \boldsymbol{e}^{(m,\varepsilon)}(\mathbf{x})\nabla\phi(\mathbf{x}) - \boldsymbol{\alpha}^{(m,\varepsilon)}(\mathbf{x})\theta(\mathbf{x})\right)\cdot\mathbf{n}\right]\right]\Big|_{\boldsymbol{x}\in\Sigma} = \mathbf{0}, \tag{6a}$$

$$[[\phi(\mathbf{x})]]|_{\boldsymbol{x}\in\Sigma} = \mathbf{0}, \quad \left[\left[\left(\tilde{\boldsymbol{e}}^{(m,\varepsilon)}(\mathbf{x})\nabla\mathbf{u}(\mathbf{x}) - \boldsymbol{\beta}^{(m,\varepsilon)}(\mathbf{x})\nabla\phi(\mathbf{x}) + \boldsymbol{\gamma}^{(m,\varepsilon)}(\mathbf{x})\theta(\mathbf{x})\right)\cdot\mathbf{n}\right]\right]\Big|_{\boldsymbol{x}\in\Sigma} = \mathbf{0}, \tag{6b}$$

$$[[\theta(\mathbf{x})]]|_{\boldsymbol{x}\in\Sigma} = \mathbf{0}, \quad \left[\left[\boldsymbol{K}^{(m,\varepsilon)}(\mathbf{x})\nabla\theta(\mathbf{x})\cdot\mathbf{n}\right]\right]\Big|_{\boldsymbol{x}\in\Sigma} = \mathbf{0}, \tag{6c}$$

being $[[f]] = f^i(\Sigma) - f^j(\Sigma)$ the jump of the values of f at the interface Σ between two different phases i and j in the periodic cell $\mathcal{A}$ and $\mathbf{n}$ the outward normal to the interface itself.

By virtue of the $\mathcal{Q}$-periodicity of the micro constitutive tensors (2) and the $\mathcal{L}$-periodicity of volume forces, all the micro fields result to be dependent on both the slow variable $\mathbf{x}$ and the fast one $\boldsymbol{\xi}$, namely

$$\mathbf{u} = \mathbf{u}\left(\mathbf{x}; \boldsymbol{\xi} = \frac{\mathbf{x}}{\varepsilon}\right), \quad \phi = \phi\left(\mathbf{x}; \boldsymbol{\xi} = \frac{\mathbf{x}}{\varepsilon}\right), \quad \theta = \theta\left(\mathbf{x}; \boldsymbol{\xi} = \frac{\mathbf{x}}{\varepsilon}\right).$$

$\mathcal{Q}$-periodicity of coefficients of equations (5a)-(5c), makes the solutions particularly complex to derive, both analytically and numerically. Therefore, it is convenient to replace the heterogeneous model with an equivalent homogeneous one, obtaining in this way equations whose coefficients are not rapidly oscillating. In what follows, the formulation of an equivalent first-order homogenized thermo-piezoelectric continuum will be presented, as derived in (Fantoni et al., 2017), and the obtained exact expressions of the overall constitutive tensors will be provided. In the equivalent homogenized medium, the macro fields for each material point $\mathbf{x}$ are the displacement field $\mathbf{U}(\mathbf{x}) = U_i\,\mathbf{e}_i$, the electric potential $\Phi(\mathbf{x})$, and the relative temperature $\Theta(\mathbf{x})$. They are $\mathcal{L}$-periodic functions dependent only on the slow variable $\mathbf{x}$.

4 Asymptotic homogenization approach to thermo-piezoelectric composites

The following down-scaling relations can be derived for the three micro-fields, representing these lasts trough an asymptotic expansions in powers of the microstructural length scale ε (Bakhvalov and Panasenko, 1984; Bensoussan et al., 1978)

$$\begin{aligned} u_k(\mathbf{x};\boldsymbol{\xi}) =& U_k(\mathbf{x}) + \varepsilon\left(N^{(1)}_{kpq_1}(\boldsymbol{\xi})\frac{\partial U_p(\mathbf{x})}{\partial x_{q_1}} + \tilde{N}^{(1)}_{kq_1}(\boldsymbol{\xi})\frac{\partial\Phi(\mathbf{x})}{\partial x_{q_1}} + \hat{N}^{(1)}_{k}\Theta(x)\right)\Big|_{\boldsymbol{\xi}=\mathbf{x}/\boldsymbol{\varepsilon}} \\ &+ \varepsilon^2\left(N^{(2)}_{kpq_1q_2}(\boldsymbol{\xi})\frac{\partial^2 U_p(\mathbf{x})}{\partial x_{q_1}\partial x_{q_2}} + \tilde{N}^{(2)}_{kq_1q_2}(\boldsymbol{\xi})\frac{\partial^2\Phi(\mathbf{x})}{\partial x_{q_1}\partial x_{q_2}} + \hat{N}^{(2)}_{kq_1}\frac{\partial\Theta(\mathbf{x})}{\partial x_{q_1}}\right)\Big|_{\boldsymbol{\xi}=\mathbf{x}/\boldsymbol{\varepsilon}} + \mathcal{O}(\varepsilon)^3, \end{aligned} \tag{7a}$$

$$\begin{aligned} \phi(\mathbf{x};\boldsymbol{\xi}) =& \phi(\mathbf{x}) + \varepsilon\left(W^{(1)}_{q_1}(\boldsymbol{\xi})\frac{\partial\Phi(\mathbf{x})}{\partial x_{q_1}} + \tilde{W}^{(1)}_{pq_1}(\boldsymbol{\xi})\frac{\partial U_p(\mathbf{x})}{\partial x_{q_1}} + \hat{W}^{(1)}(\boldsymbol{\xi})\Theta(\mathbf{x})\right)\Big|_{\boldsymbol{\xi}=\mathbf{x}/\boldsymbol{\varepsilon}} \\ &+ \varepsilon^2\left(W^{(2)}_{q_1q_2}(\boldsymbol{\xi})\frac{\partial^2\Phi(\mathbf{x})}{\partial x_{q_1}\partial x_{q_2}} + \tilde{W}^{(2)}_{pq_1q_2}(\boldsymbol{\xi})\frac{\partial^2 U_p(\mathbf{x})}{\partial x_{q_1}\partial x_{q_2}} + \hat{W}^{(2)}_{q_1}(\boldsymbol{\xi})\frac{\partial\Theta(\mathbf{x})}{\partial x_{q_1}}\right)\Big|_{\boldsymbol{\xi}=\mathbf{x}/\boldsymbol{\varepsilon}} + \mathcal{O}(\varepsilon)^3, \end{aligned} \tag{7b}$$

$$\theta(\mathbf{x};\boldsymbol{\xi}) = \Theta(\mathbf{x}) + \varepsilon\left(M^{(1)}_{q_1}(\boldsymbol{\xi})\frac{\partial\Theta(\mathbf{x})}{\partial x_{q_1}}\right)_{\boldsymbol{\xi}=\mathbf{x}/\boldsymbol{\varepsilon}} + \varepsilon^2\left(M^{(2)}_{q_1q_2}(\boldsymbol{\xi})\frac{\partial^2\Theta(\mathbf{x})}{\partial x_{q_1}\partial x_{q_2}}\right)\Big|_{\boldsymbol{\xi}=\mathbf{x}/\boldsymbol{\varepsilon}} + \mathcal{O}(\varepsilon)^3. \tag{7c}$$

Relations (7a)-(7c) have been proved in detail in (Fantoni et al., 2017). In equations (7a)-(7c), $N^{(1)}_{kpq_1}$, $\tilde{N}^{(1)}_{kq_1}$, $\hat{N}^{(1)}_{k}$, $N^{(2)}_{kpq_1q_2}$, $\tilde{N}^{(2)}_{kq_1q_2}$, $\hat{N}^{(2)}_{kq_1}$ are the perturbation functions for the micro displacement field, $W^{(1)}_{q_1}$, $\tilde{W}^{(1)}_{pq_1}$, $\hat{W}^{(1)}$, $W^{(2)}_{q_1q_2}$, $\tilde{W}^{(2)}_{pq_1q_2}$, $\hat{W}^{(2)}_{q_1}$ are the perturbation functions for the micro electric potential field, and finally $M^{(1)}_{q_1}$, $M^{(2)}_{q_1q_2}$ are the perturbation functions for the micro relative temperature field. They express the influence of the fast variable $\boldsymbol{\xi} = \mathbf{x}/\varepsilon$ on the micro fields reflecting the effects of material inhomogeneities. It is assumed

that they have vanishing mean values over the unit cell $\mathcal{Q}$ in order to assure their uniqueness. Therefore they all satisfy the following normalization condition over $\mathcal{Q}$

$$\langle\,(\cdot)\,\rangle = \frac{1}{\delta}\int_{\mathcal{Q}}(\cdot)\,d\boldsymbol{\xi} \tag{8}$$

Substituting down scaling relations (7a)-(7c) into field equations (5a)-(5c) asymptotically expanded, a series of recursive differential problems can be obtained. Field equations of the equivalent first-order thermo-piezoelectric continuum can be obtained considering only the ε^{-1} and ε^{0} terms of the sequence of PDEs derived by the asymptotic procedure, according to (Fantoni et al., 2017), exploiting the property

$$\frac{\partial}{\partial x_j}f(\mathbf{x};\boldsymbol{\xi}=\frac{\mathbf{x}}{\varepsilon}) = \left(\frac{\partial f}{\partial x_j}+\frac{1}{\varepsilon}\frac{\partial f}{\partial \xi_j}\right)\Big|_{\boldsymbol{\xi}=\frac{\mathbf{x}}{\varepsilon}} = \left(\frac{\partial f}{\partial x_j}+\frac{f_j}{\varepsilon}\right)\Big|_{\boldsymbol{\xi}=\frac{\mathbf{x}}{\varepsilon}}.$$

In order to obtain a set of PDEs with constant coefficients, the fluctuation functions must satisfy non homogeneous equations known as cell problems. Because of the structure of the obtained differential cell problems with volume forces having vanishing mean values over $\mathcal{Q}$, together with the periodicity of constitutive tensors, it can be proved that perturbation functions are $\mathcal{Q}$-periodic (Bakhvalov and Panasenko, 1984). It is worth noting that a strong coupling persists between the mechanical and the electrical problems, as can be envisaged by noting that the micro-displacement $\mathbf{u}$ and the micro-electric potential ϕ don't decouple in the microscale field equations asymptotically expanded. At the order ε^{-1} perturbation functions must satisfy the set of three cell problems presented below. $N^{(1)}_{kpq_1}$ and $\tilde{W}^{(1)}_{pq_1}$ are the solution of

$$\begin{cases} \left(C^m_{ijkl}\,N^{(1)}_{kpq_1,l}\right)_{,j} + \left(e^m_{ijk}\,\tilde{W}^{(1)}_{pq_1,k}\right)_{,j} + C^m_{ijpq_1,j} = n^{(1)}_{ipq_1} \\ \left(e^m_{kli}\,N^{(1)}_{kpq_1,l}\right)_{,i} - \left(\beta^m_{il}\tilde{W}^{(1)}_{pq_1,l}\right)_{,i} + e^m_{pq_1i,i} = \tilde{w}^{(1)}_{pq_1} \end{cases}, \tag{9}$$

with interface conditions defined at the interface Σ_1 between two different phases in the unit cell $\mathcal{Q}$

$$\begin{aligned} &\left[\left[N^{(1)}_{kpq_1}\right]\right]\Big|_{\boldsymbol{\xi}\in\Sigma_1} = 0, \\ &\left[\left[\tilde{W}^{(1)}_{pq_1}\right]\right]\Big|_{\boldsymbol{\xi}\in\Sigma_1} = 0, \\ &\left[\left[\left(C^m_{ijkl}\left(\delta_{kp}\,\delta_{lq_1}+N^{(1)}_{kpq_1,l}\right)+e^m_{ijk}\,\tilde{W}^{(1)}_{pq_1,k}\right)n_j\right]\right]\Big|_{\boldsymbol{\xi}\in\Sigma_1} = 0, \\ &\left[\left[\left(e^m_{kli}\left(\delta_{kp}\,\delta_{lq_1}+N^{(1)}_{kpq_1,l}\right)-\beta^m_{il}\,\tilde{W}^{(1)}_{pq_1,l}\right)n_i\right]\right]\Big|_{\boldsymbol{\xi}\in\Sigma_1} = 0. \end{aligned} \tag{10}$$

and normalization conditions

$$\left\langle N^{(1)}_{kpq_1}\right\rangle = \left\langle \tilde{W}^{(1)}_{pq_1}\right\rangle = 0, \tag{11}$$

as defined in (8). From the solution of the following cell problem, one can derive perturbation functions $\tilde{N}^{(1)}_{kq_1}$ and $W^{(1)}_{q_1}$

$$\begin{cases} \left(C^m_{ijkl}\,\tilde{N}^{(1)}_{kq_1,l}\right)_{,j} + \left(e^m_{ijk}\,W^{(1)}_{q_1,k}\right)_{,j} + e^m_{ijq_1,j} = \tilde{n}^{(1)}_{iq_1} \\ \left(e^m_{kli}\,\tilde{N}^{(1)}_{kq_1,l}\right)_{,i} - \left(\beta^m_{il}\,W^{(1)}_{q_1,l}\right)_{,i} - \beta^m_{iq_1,i} = w^{(1)}_{q_1} \end{cases}. \tag{12}$$

Interface conditions for the problem at hand have the form

$$\begin{aligned} &\left[\left[\tilde{N}^{(1)}_{kq_1}\right]\right]\Big|_{\boldsymbol{\xi}\in\Sigma_1} = 0, \\ &\left[\left[W^{(1)}_{q_1}\right]\right]\Big|_{\boldsymbol{\xi}\in\Sigma_1} = 0, \\ &\left[\left[\left(C^m_{ijkl}\,\tilde{N}^{(1)}_{kq_1,l}+e^m_{ijk}\left(\delta_{kq_1}+W^{(1)}_{q_1,k}\right)\right)n_j\right]\right]\Big|_{\boldsymbol{\xi}\in\Sigma_1} = 0, \\ &\left[\left[\left(e^m_{kli}\,\tilde{N}^{(1)}_{kq_1,l}-\beta^m_{il}\left(\delta_{lq_1}+W^{(1)}_{q_1,l}\right)\right)n_i\right]\right]\Big|_{\boldsymbol{\xi}\in\Sigma_1} = 0, \end{aligned} \tag{13}$$

while normalization conditions are

$$\left\langle \tilde{N}^{(1)}_{kq_1} \right\rangle = \left\langle W^{(1)}_{q_1} \right\rangle = 0. \tag{14}$$

Finally, the third electro-mechanical cell problem at the order ε^{-1} allows to derive perturbation functions $\hat{N}^{(1)}_k$ and $\hat{W}^{(1)}$

$$\begin{cases} \left(C^m_{ijkl}\,\hat{N}^{(1)}_{k,l}\right)_{,j} + \left(e^m_{ijk}\,\hat{W}^{(1)}_{,k}\right)_{,j} - \alpha^m_{ij,j} = \hat{n}^{(1)}_i \\ \left(e^m_{kli}\,\hat{N}^{(1)}_{k,l}\right)_{,i} - \left(\beta^m_{il}\hat{W}^{(1)}_{,l}\right)_{,i} + \gamma^m_{i,i} = \hat{w}^{(1)} \end{cases}. \tag{15}$$

Its interface conditions are expressed as

$$\begin{aligned} &\left[\left[\hat{N}^{(1)}_k\right]\right]\Big|_{\boldsymbol{\xi}\in\Sigma_1} = 0, \\ &\left[\left[\hat{W}^{(1)}\right]\right]\Big|_{\boldsymbol{\xi}\in\Sigma_1} = 0, \\ &\left[\left[\left(C^m_{ijkl}\,\hat{N}^{(1)}_{k,l} + e^m_{ijk}\,\hat{W}^{(1)}_{,k} - \alpha^m_{ij}\right) n_j\right]\right]\Big|_{\boldsymbol{\xi}\in\Sigma_1} = 0, \\ &\left[\left[\left(e^m_{kli}\,\hat{N}^{(1)}_{k,l} - \beta^m_{il}\hat{W}^{(1)}_{,l} + \gamma^m_i\right) n_i\right]\right]\Big|_{\boldsymbol{\xi}\in\Sigma_1} = 0, \end{aligned} \tag{16}$$

and normalization conditions are

$$\left\langle \hat{N}^{(1)}_k \right\rangle = \left\langle \hat{W}^{(1)} \right\rangle = 0. \tag{17}$$

Solvability condition of problems (9), (12), and (15) in the class of $\mathcal{Q}$-periodic functions (Bakhvalov and Panasenko, 1984), together with respective interface conditions (10), (13), and (16) implies that

$$\begin{aligned} &n^{(1)}_{ipq_1} = \left\langle C^m_{ijpq_1,j} \right\rangle = 0, \quad \tilde{w}^{(1)}_{pq_1} = \left\langle e^m_{pq_1 i,i} \right\rangle = 0, \quad \tilde{n}^{(1)}_{iq_1} = \left\langle e^m_{ijq_1,j} \right\rangle = 0, \\ &w^{(1)}_{q_1} = \left\langle -\beta^m_{iq_1,i} \right\rangle = 0, \quad \hat{n}^{(1)}_i = \left\langle -\alpha^m_{ij,j} \right\rangle = 0, \quad \hat{w}^{(1)} = \left\langle \gamma^m_{i,i} \right\rangle = 0. \end{aligned} \tag{18}$$

Heat diffusion cell problem at the order ε^{-1} provides perturbation function $M^{(1)}_{q_1}$. It holds

$$\left(K^m_{ij}\,M^{(1)}_{q_1,j}\right)_{,i} + K^m_{iq_1,i} = m^{(1)}_{q_1}. \tag{19}$$

Its interface conditions have the following form

$$\begin{aligned} &\left[\left[M^{(1)}_{q_1}\right]\right]\Big|_{\boldsymbol{\xi}\in\Sigma_1} = 0, \\ &\left[\left[K^m_{ij}\left(M^{(1)}_{q_1,j} + \delta_{jq_1}\right) n_i\right]\right]\Big|_{\boldsymbol{\xi}\in\Sigma_1} = 0, \end{aligned} \tag{20}$$

while normalization condition is

$$\left\langle M^{(1)}_{q_1} \right\rangle = 0. \tag{21}$$

Due to the $\mathcal{Q}$-periodicity of components $K^m_{iq_1}$, one has

$$m^{(1)}_{q_1} = \left\langle K^m_{iq_1,i} \right\rangle = 0 \tag{22}$$

for the solvability of differential problem (19) with interface conditions (20). Once perturbation functions involved in cell problem (9), (12), (15), and (19) at the order ε^{-1} are determined, one can solve the cell problems at the order ε^0, derived from equations (5a)-(5c). Specifically, perturbation functions $N^{(2)}_{kpq_1q_2}$ and $\tilde{W}^{(2)}_{pq_1q_2}$ are the solution of the suitably symmetrized cell problem which guarantees $N^{(2)}_{kpq_1q_2} = N^{(2)}_{kpq_2q_1}$ and

$\tilde{W}^{(2)}_{pq_1q_2} = \tilde{W}^{(2)}_{pq_2q_1}$ and that has the following form

$$\begin{cases} \left(C^m_{ijkl}\, N^{(2)}_{kpq_1q_2,l}\right)_{,j} + \left(e^m_{ijk}\, \tilde{W}^{(2)}_{pq_1q_2,k}\right)_{,j} + \frac{1}{2}\left[\left(C^m_{ijkq_2}\, N^{(1)}_{kpq_1}\right)_{,j} + C^m_{iq_1pq_2} + C^m_{iq_2kl}\, N^{(1)}_{kpq_1,l} + \right. \\ + \left(e^m_{ijq_2}\, \tilde{W}^{(1)}_{pq_1}\right)_{,j} + e^m_{iq_2k}\, \tilde{W}^{(1)}_{pq_1,k} + \left(C^m_{ijkq_1}\, N^{(1)}_{kpq_2}\right)_{,j} + C^m_{iq_2pq_1} + C^m_{iq_1kl}\, N^{(1)}_{kpq_2,l} + \left(e^m_{ijq_1}\, \tilde{W}^{(1)}_{pq_2}\right)_{,j} + \\ \left. + e^m_{iq_1k}\, \tilde{W}^{(1)}_{pq_2,k}\right] = n^{(2)}_{ipq_1q_2}, \\ \\ \left(e^m_{kli}\, N^{(2)}_{kpq_1q_2,l}\right)_{,i} - \left(\beta^m_{il}\, \tilde{W}^{(2)}_{pq_1q_2,l}\right)_{,i} + \frac{1}{2}\left[\left(e^m_{kq_2i}\, N^{(1)}_{kpq_1}\right)_{,i} + e^m_{klq_2} N^{(1)}_{kpq_1,l} + e^m_{pq_2q_1} + \right. \\ - \left(\beta^m_{iq_2}\, \tilde{W}^{(1)}_{pq_1}\right)_{,i} - \beta^m_{q_2l}\, \tilde{W}^{(1)}_{pq_1,l} + \left(e^m_{kq_1i}\, N^{(1)}_{kpq_2}\right)_{,i} + e^m_{klq_1}\, N^{(1)}_{kpq_2,l} + e^m_{pq_1q_2} - \left(\beta^m_{iq_1}\, \tilde{W}^{(1)}_{pq_2}\right)_{,i} + \\ \left. - \beta^m_{q_1l}\, \tilde{W}^{(1)}_{pq_2,l}\right] = \tilde{w}^{(2)}_{pq_1q_2} \end{cases} \tag{23}$$

Relative interface conditions are

$$\begin{aligned} &\left[\left[N^{(2)}_{kpq_1q_2}\right]\right]\Big|_{\boldsymbol{\xi}\in\Sigma_1} = 0, \\ &\left[\left[\tilde{W}^{(2)}_{pq_1q_2}\right]\right]\Big|_{\boldsymbol{\xi}\in\Sigma_1} = 0, \\ &\left[\left[\left(C^m_{ijkl}\, N^{(2)}_{kpq_1q_2,l} + e^m_{ijk}\, \tilde{W}^{(2)}_{pq_1q_2,k} + \frac{1}{2}\left(C^m_{ijkq_2}\, N^{(1)}_{kpq_1} + C^m_{ijkq_1}\, N^{(1)}_{kpq_2} + e^m_{ijq_2}\, \tilde{W}^{(1)}_{pq_1} + e^m_{ijq_1}\, \tilde{W}^{(1)}_{pq_2}\right)\right) n_j\right]\right]\Big|_{\boldsymbol{\xi}\in\Sigma_1} = 0, \\ &\left[\left[\left(e^m_{kli}\, N^{(2)}_{kpq_1q_2,l} - \beta^m_{il}\, \tilde{W}^{(2)}_{pq_1q_2,l} + \frac{1}{2}\left(e^m_{kq_2i}\, N^{(1)}_{kpq_1} - \beta^m_{iq_2}\, \tilde{W}^{(1)}_{pq_1} + e^m_{kq_1i}\, N^{(1)}_{kpq_2} - \beta^m_{iq_1}\, \tilde{W}^{(1)}_{pq_2}\right)\right) n_i\right]\right]\Big|_{\boldsymbol{\xi}\in\Sigma_1} = 0, \end{aligned} \tag{24}$$

while normalization conditions are expressed as

$$\left\langle N^{(2)}_{kpq_1q_2}\right\rangle = \left\langle \tilde{W}^{(2)}_{pq_1q_2}\right\rangle = 0. \tag{25}$$

The second electro-mechanical cell problem at the order ε^0, which provides perturbation functions $\tilde{N}^{(2)}_{kq_1q_2}$ and $W^{(2)}_{q_1q_2}$, can be expressed in the following form symmetrized, once again, with respect to indices q_1 and q_2

$$\begin{cases} \left(C^m_{ijkl}\, \tilde{N}^{(2)}_{kq_1q_2,l}\right)_{,j} + \left(e^m_{ijk}\, W^{(2)}_{q_1q_2,k}\right)_{,j} + \frac{1}{2}\left[\left(C^m_{ijkq_2}\, \tilde{N}^{(1)}_{kq_1}\right)_{,j} + C^m_{iq_2kl}\, \tilde{N}^{(1)}_{kq_1,l} + \left(e^m_{ijq_2}\, W^{(1)}_{q_1}\right)_{,j} + \right. \\ + e^m_{iq_1q_2} + e^m_{iq_2k}\, W^{(1)}_{q_1,k} + \left(C^m_{ijkq_1}\, \tilde{N}^{(1)}_{kq_2}\right)_{,j} + C^m_{iq_1kl}\, \tilde{N}^{(1)}_{kq_2,l} + \left(e^m_{ijq_1}\, W^{(1)}_{q_2}\right)_{,j} + e_{iq_2q_1} + e^m_{iq_1k}\, W^{(1)}_{q_2,k}\Big] = \\ = \tilde{n}^{(2)}_{iq_1q_2} \\ \\ \left(e^m_{kli}\, \tilde{N}^{(2)}_{kq_1q_2,l}\right)_{,i} - \left(\beta^m_{il}\, W^{(2)}_{q_1q_2,l}\right)_{,i} + \frac{1}{2}\left[\left(e^m_{kq_2i}\, \tilde{N}^{(1)}_{kq_1}\right)_{,i} + e^m_{klq_2}\, \tilde{N}^{(1)}_{kq_1,l} - \left(\beta^m_{iq_2} W^{(1)}_{q_1}\right)_{,i} - \beta^m_{q_1q_2} + \right. \\ - \beta^m_{q_2l}\, W^{(1)}_{q_1,l} + \left(e^m_{kq_1i}\, \tilde{N}^{(1)}_{kq_2}\right)_{,i} + e^m_{klq_1}\, \tilde{N}^{(1)}_{kq_2,l} - \left(\beta^m_{iq_1}\, W^{(1)}_{q_2}\right)_{,i} - \beta^m_{q_2q_1} - \beta^m_{q_1l}\, W^{(1)}_{q_2,l}\Big] = \\ = w^{(2)}_{q_1q_2} \end{cases} \tag{26}$$

Interface conditions for the problem at hand are

$$\begin{aligned} &\left[\left[\tilde{N}^{(2)}_{kq_1q_2}\right]\right]\Big|_{\boldsymbol{\xi}\in\Sigma_1} = 0, \\ &\left[\left[W^{(2)}_{q_1q_2}\right]\right]\Big|_{\boldsymbol{\xi}\in\Sigma_1} = 0, \\ &\left[\left[\left\{C^m_{ijkl}\, \tilde{N}^{(2)}_{kq_1q_2,l} + e^m_{ijk}\, W^{(2)}_{q_1q_2,k} + \frac{1}{2}\left(C^m_{ijkq_2}\, \tilde{N}^{(1)}_{kq_1} + e^m_{ijq_2}\, W^{(1)}_{q_1} + C^m_{ijkq_1}\, \tilde{N}^{(1)}_{kq_2} + e^m_{ijq_1}\, W^{(1)}_{q_2}\right)\right\} n_j\right]\right]\Big|_{\boldsymbol{\xi}\in\Sigma_1} = 0, \end{aligned}$$

$$\left[\left[\left\{e^m_{kli}\,\tilde{N}^{(2)}_{kq_1q_2,l}-\beta^m_{il}\,W^{(2)}_{q_1q_2,l}+\frac{1}{2}\left(e^m_{kq_2i}\,\tilde{N}^{(1)}_{kq_1}-\beta^m_{iq_2}\,W^{(1)}_{q_1}+e^m_{kq_1i}\,\tilde{N}^{(1)}_{kq_2}-\beta^m_{iq_1}\,W^{(1)}_{q_2}\right)\right\}n_i\right]\right]\Big|_{\boldsymbol{\xi}\in\Sigma_1}=0, \tag{27}$$

and normalization conditions have the form

$$\left\langle \tilde{N}^{(2)}_{kq_1q_2}\right\rangle=\left\langle W^{(2)}_{q_1q_2}\right\rangle=0. \tag{28}$$

Finally, perturbation functions $\hat{N}^{(2)}_{kq_1}$ and $\hat{W}^{(2)}_{q_1}$ are provided by the solution of the third piezoelectric cell problem at the order ε^0

$$\begin{cases}\left(C^m_{ijkl}\,\hat{N}^{(2)}_{kq_1,l}\right)_{,j}+\left(e^m_{ijk}\,\hat{W}^{(2)}_{q_1,k}\right)_{,j}+\left(C^m_{ijkq_1}\,\hat{N}^{(1)}_{k}\right)_{,j}+C^m_{iq_1kl}\,\hat{N}^{(1)}_{k,l}+\left(e^m_{ijq_1}\,\hat{W}^{(1)}\right)_{,j}+\\ +e^m_{iq_1k}\,\hat{W}^{(1)}_{,k}-\left(\alpha^m_{ij}\,M^{(1)}_{q_1}\right)_{,j}-\alpha^m_{iq_1}=\hat{n}^{(2)}_{iq_1}\\ \\ \left(e^m_{kli}\,\hat{N}^{(2)}_{kq_1,l}\right)_{,i}-\left(\beta^m_{il}\,\hat{W}^{(2)}_{q_1,l}\right)_{,i}+\left(e^m_{kq_1i}\,\hat{N}^{(1)}_{k}\right)_{,i}+e^m_{klq_1}\,\hat{N}^{(1)}_{k,l}-\left(\beta^m_{iq_1}\,\hat{W}^{(1)}\right)_{,i}+\\ -\beta^m_{q_1l}\,\hat{W}^{(1)}_{,l}+\left(\gamma^m_i\,M^{(1)}_{q_1}\right)_{,i}+\gamma^m_{q_1}=\hat{w}^{(2)}_{q_2}\end{cases}. \tag{29}$$

Relative interface conditions have the following form

$$\begin{aligned}&\left[\left[\hat{N}^{(2)}_{kq_1}\right]\right]\Big|_{\boldsymbol{\xi}\in\Sigma_1}=0,\\ &\left[\left[\hat{W}^{(2)}_{q_1}\right]\right]\Big|_{\boldsymbol{\xi}\in\Sigma_1}=0,\\ &\left[\left[\left(C^m_{ijkl}\,\hat{N}^{(2)}_{kq_1,l}+e^m_{ijk}\,\hat{W}^{(2)}_{q_1,k}+C^m_{ijkq_1}\,\hat{N}^{(1)}_{k}+e^m_{ijq_1}\,\hat{W}^{(1)}-\alpha^m_{ij}\,M^{(1)}_{q_1}\right)n_j\right]\right]\Big|_{\boldsymbol{\xi}\in\Sigma_1}=0,\\ &\left[\left[\left(e^m_{kli}\,\hat{N}^{(2)}_{kq_1,l}-\beta^m_{il}\,\hat{W}^{(2)}_{q_1,l}+e^m_{kq_1i}\,\hat{N}^{(1)}_{k}-\beta^m_{iq_1}\,\hat{W}^{(1)}+\gamma^m_i\,M^{(1)}_{q_1}\right)n_i\right]\right]\Big|_{\boldsymbol{\xi}\in\Sigma_1}=0,\end{aligned} \tag{30}$$

and normalization conditions are

$$\left\langle \hat{N}^{(2)}_{kq_1}\right\rangle=\left\langle \hat{W}^{(2)}_{q_1}\right\rangle=0. \tag{31}$$

One has

$$n^{(2)}_{ipq_1q_2}=\frac{1}{2}\left\langle C^m_{iq_1pq_2}+C^m_{iq_2kl}\,N^{(1)}_{kpq_1,l}+e^m_{iq_2k}\,\tilde{W}^{(1)}_{pq_1,k}+C^m_{iq_2pq_1}+C^m_{iq_1kl}\,N^{(1)}_{kpq_2,l}+e^m_{iq_1k}\,\tilde{W}^{(1)}_{pq_2,k}\right\rangle, \tag{32a}$$

$$\tilde{w}^{(2)}_{pq_1q_2}=\frac{1}{2}\left\langle e^m_{klq_2}\,N^{(1)}_{kpq_1,l}+e^m_{pq_2q_1}-\beta^m_{q_2l}\,\tilde{W}^{(1)}_{pq_1,l}+e^m_{klq_1}\,N^{(1)}_{kpq_2,l}+e^m_{pq_1q_2}-\beta^m_{q_1l}\,\tilde{W}^{(1)}_{pq_2,l}\right\rangle, \tag{32b}$$

$$\tilde{n}^{(2)}_{iq_1q_2}=\frac{1}{2}\left\langle C^m_{iq_2kl}\,\tilde{N}^{(1)}_{kq_1,l}+e_{iq_1q_2}+e^m_{iq_2k}\,W^{(1)}_{q_1,k}+C^m_{iq_1kl}\,\tilde{N}^{(1)}_{kq_2,l}+e^m_{iq_2q_1}+e^m_{iq_1k}\,W^{(1)}_{q_2,k}\right\rangle, \tag{32c}$$

$$w^{(2)}_{q_1q_2}=\frac{1}{2}\left\langle e^m_{klq_2}\,\tilde{N}^{(1)}_{kq_1,l}-\beta^m_{q_1q_2}-\beta^m_{q_2l}\,W^{(1)}_{q_1,l}+e^m_{klq_1}\,\tilde{N}^{(1)}_{kq_2,l}-\beta^m_{q_2q_1}-\beta^m_{q_1l}\,W^{(1)}_{q_2,l}\right\rangle, \tag{32d}$$

$$\hat{n}^{(2)}_{iq_1}=\left\langle C^m_{iq_1kl}\,\hat{N}^{(1)}_{k,l}+e_{iq_1k}\,\hat{W}^{(1)}_{,k}-\alpha^{(m)}_{iq_1}\right\rangle, \tag{32e}$$

$$\hat{w}^{(2)}_{q_2}=\left\langle e^m_{klq_1}\,\hat{N}^{(1)}_{k,l}-\beta^m_{q_1l}\,\hat{W}^{(1)}_{,l}+\gamma^m_{q_1}\right\rangle. \tag{32f}$$

Heat diffusion problem at the order ε^0 provides perturbation function $M^{(2)}_{q_1q_2}$ and has the form

$$\left(K^m_{ij}\,M^{(2)}_{q_1q_2,j}\right)_{,i}+\frac{1}{2}\left[\left(K^m_{iq_2}\,M^{(1)}_{q_1}\right)_{,i}+K^m_{q_1q_2}+K^m_{q_2j}\,M^{(1)}_{q_1,j}+\left(K^m_{iq_2}\,M^{(1)}_{q_2}\right)_{,i}+K^m_{q_2q_1}+K^m_{q_1j}\,M^{(1)}_{q_2,j}\right]=m^{(2)}_{q_1q_2}, \tag{33}$$

with interface conditions expressed as

$$\left[\left[M^{(2)}_{q_1q_2}\right]\right]\Big|_{\boldsymbol{\xi}\in\Sigma_1}=0,$$

$$\left[\left[K_{ij}^{m}\left(M_{q_1q_2,j}^{(2)}+\frac{1}{2}\left(\delta_{jq_2}\,M_{q_1}^{(1)}+\delta_{jq_1}\,M_{q_2}^{(1)}\right)\right)n_i\right]\right]\Big|_{\boldsymbol{\xi}\in\Sigma_1}=0, \tag{34}$$

and normalization condition

$$\left\langle M_{q_1q_2}^{(2)}\right\rangle=0. \tag{35}$$

Term $m_{q_1q_2}^{(2)}$ results to be

$$m_{q_1q_2}^{(2)}=\frac{1}{2}\left\langle\, K_{q_1q_2}^{m}+K_{q_2j}^{m}\,M_{q_1,j}^{(1)}+K_{q_2q_1}^{m}+K_{q_1j}^{m}\,M_{q_2,j}^{(1)}\,\right\rangle \tag{36}$$

For the solvability conditions, the constants (32a)-(32f) and (36) are determined once again by imposing the non homogeneous terms in equation (23), (26), (29), and (33) possess vanishing mean values over the unit cell $\mathcal{Q}$. This implies the $\mathcal{Q}$-periodicity of perturbation functions and guarantees the continuity and regularity of the micro-fields u_k, ϕ and θ. Once perturbation functions are known from the resolution of cell problems, the following averaged field equations can be derived, exploiting asymptotic expansions (7a)-(7c) and truncating these lasts at the order ε^0

$$n_{ipq_1q_2}^{(2)}\frac{\partial^2U_p(\mathbf{x})}{\partial x_{q_1}\partial x_{q_2}}+\tilde{n}_{iq_1q_2}^{(2)}\frac{\partial^2\Phi(\mathbf{x})}{\partial x_{q_1}\partial x_{q_2}}-\hat{n}_{iq_1}^{(2)}\frac{\partial\Theta(\mathbf{x})}{\partial x_{q_1}}+b_i(\mathbf{x})+\mathcal{O}(\varepsilon)=0, \tag{37a}$$

$$\tilde{w}_{pq_1q_2}^{(2)}\frac{\partial^2U_p(\mathbf{x})}{\partial x_{q_1}\partial x_{q_2}}-w_{q_1q_2}^{(2)}\frac{\partial^2\Phi(\mathbf{x})}{\partial x_{q_1}\partial x_{q_2}}+\hat{w}_{q_1}^{(2)}\frac{\partial\Theta(\mathbf{x})}{\partial x_{q_1}}-\rho_e(\mathbf{x})+\mathcal{O}(\varepsilon)=0, \tag{37b}$$

$$m_{q_1q_2}^{(2)}\frac{\partial^2\Theta(\mathbf{x})}{\partial x_{q_1}\partial x_{q_2}}+r(\mathbf{x})+\mathcal{O}(\varepsilon)=0. \tag{37c}$$

Normalization conditions

$$\frac{1}{\delta L^2}\int_{\mathcal{L}}U_p\left(\mathbf{x}\right)d\mathbf{x}=0,\quad\frac{1}{\delta L^2}\int_{\mathcal{L}}\Phi\left(\mathbf{x}\right)d\mathbf{x}=0,\quad\frac{1}{\delta L^2}\int_{\mathcal{L}}\Theta\left(\mathbf{x}\right)d\mathbf{x}=0. \tag{38}$$

are required to be fulfilled by the $\mathcal{L}$-periodic macroscopic solutions $\mathbf{U}(\mathbf{x}),\Phi(\mathbf{x})$, and $\Theta(\mathbf{x})$ of differential problems (37).
Average field equations (37) are solved by means of an asymptotic expansion of the macro-fields in powers of ε:

$$U_k(\mathbf{x})=\sum_{j=0}^{+\infty}\varepsilon^j\,U_k^{(j)}(\mathbf{x}), \tag{39a}$$

$$\Phi(\mathbf{x})=\sum_{j=0}^{+\infty}\varepsilon^j\,\Phi^{(j)}(\mathbf{x}), \tag{39b}$$

$$\Theta(\mathbf{x})=\sum_{j=0}^{+\infty}\varepsilon^j\,\Theta^{(j)}(\mathbf{x}). \tag{39c}$$

A series of recursive differential problems in terms of $U_k^{(j)}$, $\Phi^{(j)}$, and $\Theta^{(j)}$ can be obtained substituting expansions (39) into (37). Truncating expansions (39) at the zeroth order, the governing equations of the equivalent first-order (Cauchy) homogenized continuum can be obtained. They can be written in terms of the components $C_{iq_1pq_2}$, $\beta_{q_1q_2}$, $K_{q_1q_2}$, $e_{iq_1q_2}$, α_{iq_1}, and γ_{q_1} of the overall constitutive tensors as

$$C_{iq_1pq_2}\frac{\partial^2U_p(\mathbf{x})}{\partial x_{q_1}\partial x_{q_2}}+e_{iq_1q_2}\frac{\partial^2\Phi(\mathbf{x})}{\partial x_{q_1}\partial x_{q_2}}-\alpha_{iq_1}\frac{\partial\Theta(\mathbf{x})}{\partial x_{q_1}}+b_i(\mathbf{x})=0, \tag{40a}$$

$$e_{pq_1q_2}\frac{\partial^2U_p(\mathbf{x})}{\partial x_{q_1}\partial x_{q_2}}-\beta_{q_1q_2}\frac{\partial^2\Phi(\mathbf{x})}{\partial x_{q_1}\partial x_{q_2}}+\gamma_{q_1}\frac{\partial\Theta(\mathbf{x})}{\partial x_{q_1}}-\rho_e(\mathbf{x})=0, \tag{40b}$$

$$K_{q_1q_2}\frac{\partial^2\Theta(\mathbf{x})}{\partial x_{q_1}\partial x_{q_2}}+r(\mathbf{x})=0. \tag{40c}$$

As detailed in (Fantoni et al., 2017) components of tensors $\boldsymbol{n}^{(2)}$, $\boldsymbol{w}^{(2)}$, $\boldsymbol{m}^{(2)}$, $\tilde{\boldsymbol{n}}^{(2)}$, and $\tilde{\boldsymbol{w}}^{(2)}$, as expressed in equations (32) and (36), are related to the components of the corresponding overall constitutive tensors $\mathbb{C}, \boldsymbol{\beta}, \boldsymbol{K}$, and $\boldsymbol{e}$, in the following manner

$$n^{(2)}_{ipq_1q_2} = \frac{1}{2}\left(C_{pq_1iq_2} + C_{pq_2iq_1}\right), \quad w^{(2)}_{q_1q_2} = \beta_{q_1q_2}, \quad m^{(2)}_{q_1q_2} = K_{q_1q_2}, \quad \tilde{n}^{(2)}_{iq_1q_2} = \tilde{w}^{(2)}_{iq_1q_2} = e_{iq_1q_2}.$$

$\boldsymbol{n}^{(2)}$, $\boldsymbol{w}^{(2)}$ and $\boldsymbol{m}^{(2)}$ are symmetric and positive definite tensors, as proved in detail in (Fantoni et al., 2017). Furthermore, components of tensors $\tilde{\boldsymbol{n}}^{(2)}$ and $\tilde{\boldsymbol{w}}^{(2)}$ are proved to be identical in the above cited paper.

5 Application of asymptotic homogenization technique to microstructured thermo-piezoelectric bender actuators

In the present *Section* deflection of multilayered microstructured bender actuators is investigated in relation to some geometric parameters. In particular, unimorph and bimorph thermo-piezoelectric benders are considered (see figure 3); the first one made of an active PZT layer and a composite layer, while the second one made of two PZT laminae and a central composite stratum sandwiched among the two active layers. In both cases, the composite layer is characterized by a periodic microstructure, with PZT inclusions immersed in a polymeric matrix. Electrodes are present on the upper and lower surfaces of each active PZT lamina, as illustrated in figure 3 with a thick black line. As depicted in figure 3, benders are electrically charged by means of an imposed voltage $\Delta\Phi$ between each couple of electrodes. Furthermore, in order to exploit the pyroelectric properties of the PZT, benders are considered subject to a relative temperature gradient $\Delta\Theta$ between the extrados of the actuators, characterized by the relative temperature Θ_{ext}, and the intrados of the devices, which is at relative temperature Θ_{int}. In *Section 5.1* constitutive tensors relative to the materials constituting the benders at the microscale are provided, together with microscopic constitutive equations describing plane strain and plane stress conditions. *Section 5.2* is devoted to perform the asymptotic homogenization, as previously described in *Section 4*, of the microstructured composite layer of the benders, where inclusions with different topologies are considered. Investigated actuators remain heterogeneous at the mesoscale and made by one/two PZT laminae and one homogenized composite layer. Perturbation functions are determined as solutions of non homogeneous cell problems at the order ε^{-1} and the overall constitutive tensors of the first-order (Cauchy) homogenized medium are computed for the case at hand.
Finally, in *Section 5.3* deflection of unimorph and bimorph benders is numerically investigated under different loading conditions, in order to analyze the role of the microstructure on the stiffness of the whole actuator.

5.1 Microscopic constitutive tensors and in plane description

Consider a unimorph bender as the one depicted in figure 3-(a), formed by a pyroelectric layer and a composite layer. The pyroelectric layer is made by Lead Zirconate Titanate (PZT-5H), which has marked piezoelectric and pyroelectric properties. Such a material is considered polarized in the x_2 direction and it is characterized by the following constitutive tensors (Guo et al., 2003; Kommepalli et al., 2010; Malmonge et al., 2003; Umemiya et al., 2006; Yang, 2004), accordingly to the notation detailed in Appendix A, where symbol $|_{x_i}$ refers to the i^{th} polarization direction

$$\mathbb{C}_{PZT|x_2} = \begin{pmatrix} 12.6 & 8.41 & 7.95 & 0 & 0 & 0 \\ 8.41 & 11.7 & 8.41 & 0 & 0 & 0 \\ 7.95 & 8.41 & 12.6 & 0 & 0 & 0 \\ 0 & 0 & 0 & 2\cdot 2.3 & 0 & 0 \\ 0 & 0 & 0 & 0 & 2\cdot 2.3 & 0 \\ 0 & 0 & 0 & 0 & 0 & 2\cdot 2.3 \end{pmatrix} 10^{10}\,\frac{\mathrm{N}}{\mathrm{m}^2},$$

$$\boldsymbol{\beta}_{PZT|x_2} = \begin{pmatrix} 1.505 & 0 & 0 \\ 0 & 1.302 & 0 \\ 0 & 0 & 1.505 \end{pmatrix} 10^{-8}\,\frac{\mathrm{C}}{\mathrm{V\,m}}, \qquad \boldsymbol{K}_{PZT|x_2} = \begin{pmatrix} 1.5 & 0 & 0 \\ 0 & 1.5 & 0 \\ 0 & 0 & 1.5 \end{pmatrix} \frac{\mathrm{W}}{\mathrm{m\,K}},$$

$$\tilde{\boldsymbol{e}}_{PZT|x_2} = \begin{pmatrix} 0 & 0 & 0 & \sqrt{2}\cdot 17 & 0 & 0 \\ -6.5 & 23.3 & 0 & 0 & 0 & 0 \\ 0 & 0 & 0 & 0 & 0 & 0 \end{pmatrix} \frac{\mathrm{C}}{\mathrm{m}^2},$$

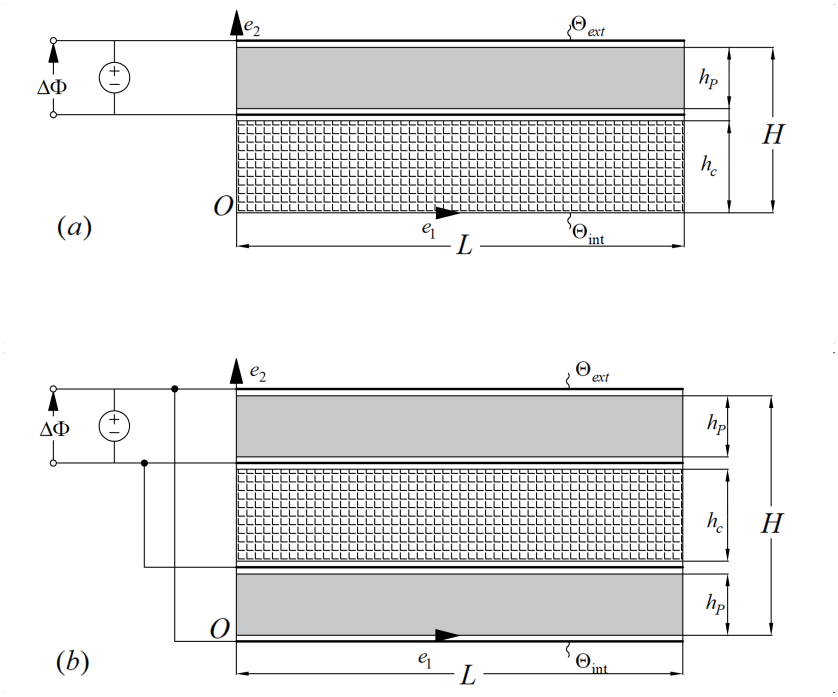

Figure 3: *Bender actuators with height H and length L: unimorph (a) and bimorph (b). PZT laminae, with thickness h_P, are represented by grey uniform color, while composite layer, with thickness h_c, is depicted with a checked background. Electrods are indicated with a thick black line. Benders are loaded by voltage $\Delta\Phi$ and relative temperature gradient $\Delta\Theta = \Theta_{ext} - \Theta_{int}$.*

$$\boldsymbol{\alpha}_{PZT|x_2} = \begin{pmatrix} 1.71 \\ 1.71 \\ 1.71 \\ 0 \\ 0 \\ 0 \end{pmatrix} 10^6 \, \frac{\mathrm{N}}{\mathrm{m^2\,K}}, \qquad \boldsymbol{\gamma}_{PZT|x_2} = \begin{pmatrix} 5 \\ 5 \\ 5 \end{pmatrix} 10^{-4} \, \frac{\mathrm{C}}{\mathrm{m^2}\,K}. \tag{41}$$

The composite layer has a micro-structure where PZT fibers, polarized in the x_3 direction, are immersed in a polymeric matrix. Fibers having circular or square/rectangular cross section have been considered, as depicted in figure 4, whose constitutive tensors are (Yang, 2004)

$$\begin{aligned}
\mathbb{C}_{PZT|x_3} &= \begin{pmatrix} 12.6 & 7.95 & 8.41 & 0 & 0 & 0 \\ 7.95 & 12.6 & 8.41 & 0 & 0 & 0 \\ 8.41 & 8.41 & 11.7 & 0 & 0 & 0 \\ 0 & 0 & 0 & 2 \cdot 2.3 & 0 & 0 \\ 0 & 0 & 0 & 0 & 2 \cdot 2.3 & 0 \\ 0 & 0 & 0 & 0 & 0 & 2 \cdot 2.3 \end{pmatrix} 10^{10} \, \frac{\mathrm{N}}{\mathrm{m^2}}, \\
\boldsymbol{\beta}_{PZT|x_3} &= \begin{pmatrix} 1.505 & 0 & 0 \\ 0 & 1.505 & 0 \\ 0 & 0 & 1.302 \end{pmatrix} 10^{-8} \, \frac{\mathrm{C}}{\mathrm{V\,m}}, \\
\tilde{\boldsymbol{e}}_{PZT|x_3} &= \begin{pmatrix} 0 & 0 & 0 & 0 & \sqrt{2} \cdot 17 & 0 \\ 0 & 0 & 0 & \sqrt{2} \cdot 17 & 0 & 0 \\ -6.5 & -6.5 & 23.3 & 0 & 0 & 0 \end{pmatrix} \frac{\mathrm{C}}{\mathrm{m^2}},
\end{aligned} \tag{42}$$

Tensors $\boldsymbol{K}_{PZT|x_3}, \boldsymbol{\alpha}_{PZT|x_3}$ and $\boldsymbol{\gamma}_{PZT|x_3}$ are the same as the ones detailed in equation (41).

Polymeric matrix is considered made of low density polyethylene (LDP), which has negligible piezoelectric and pyroelectric properties (i.e. $\boldsymbol{e}_{LDP} = \boldsymbol{0}$ and $\boldsymbol{\gamma}_{LDP} = \boldsymbol{0}$) and it is characterized by the following constitutive

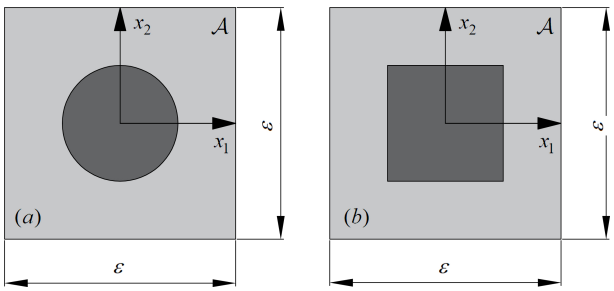

Figure 4: *Periodic cell $\mathcal{A}$ with PZT inclusions (dark grey) immersed in a low density polyethylene matrix (light grey):(a) circular inclusion, (b) square inclusion*

tensors (Peacock, 2000)

$$\mathbb{C}_{LDP} = \begin{pmatrix} 3.69 & 2.46 & 2.46 & 0 & 0 & 0 \\ 2.46 & 3.69 & 2.46 & 0 & 0 & 0 \\ 8.41 & 2.46 & 3.69 & 0 & 0 & 0 \\ 0 & 0 & 0 & 2 \cdot 0.61 & 0 & 0 \\ 0 & 0 & 0 & 0 & 2 \cdot 0.61 & 0 \\ 0 & 0 & 0 & 0 & 0 & 2 \cdot 0.61 \end{pmatrix} 10^8 \, \frac{\mathrm{N}}{\mathrm{m}^2},$$

$$\boldsymbol{\beta}_{LDP} = \begin{pmatrix} 2.04 & 0 & 0 \\ 0 & 2.04 & 0 \\ 0 & 0 & 2.04 \end{pmatrix} 10^{-11} \, \frac{\mathrm{C}}{\mathrm{V\,m}}, \qquad \boldsymbol{K}_{LDP} = \begin{pmatrix} 0.42 & 0 & 0 \\ 0 & 0.42 & 0 \\ 0 & 0 & 0.42 \end{pmatrix} \frac{\mathrm{W}}{\mathrm{m\,K}},$$

$$\boldsymbol{\alpha}_{LDP} = \begin{pmatrix} 1.03 \\ 1.03 \\ 1.03 \\ 0 \\ 0 \\ 0 \end{pmatrix} 10^5 \, \frac{\mathrm{N}}{\mathrm{m}^2\,\mathrm{K}}, \tag{43}$$

Bimorph bender (see figure 3-(b)) is formed by a central layer made of low density polyethylene and PZT fibers polarized in the x_3 direction whose constitutive tensors are described respectively in equations (43) and (42). On the upper and lower surfaces of the composite layer there are two PZT layers polarized in the x_2 direction, having constitutive properties described in equation (41). Unimorph and bimorph benders as the ones previously described have been analyzed considering plane strain and plane stress conditions. In the case of plane strain conditions, the gradients of all cinematic variables in the x_3 direction have vanishing values, namely

$$\varepsilon_{33} = \varepsilon_{13} = \varepsilon_{23} = 0, \qquad E_3 = 0, \qquad \theta_{,3} = 0.$$

In such conditions, components of the stress tensors are expressed as

$$\begin{aligned} \sigma_{11} &= C_{1111}\varepsilon_{11} + C_{1122}\varepsilon_{22} - \alpha_{11}\theta, \qquad \sigma_{22} = C_{2222}\varepsilon_{22} + C_{2211}\varepsilon_{11} - \alpha_{22}\theta, \\ \sigma_{33} &= C_{1133}\varepsilon_{11} + C_{2233}\varepsilon_{22} - \alpha_{33}\theta, \qquad \sigma_{12} = 2\,C_{1212}\varepsilon_{12}, \\ \sigma_{13} &= e_{131}\phi_{,1}, \qquad \sigma_{23} = e_{232}\phi_{,2}. \end{aligned} \tag{44}$$

Electric displacement $\mathbf{D}$ results

$$D_1 = -\beta_{11}\phi_{,1} + \gamma_1\theta, \qquad D_2 = -\beta_{22}\phi_{,2} + \gamma_2\theta, \qquad D_3 = \tilde{e}_{311}\varepsilon_{11} + \tilde{e}_{322}\varepsilon_{22} + \gamma_3\theta, \tag{45}$$

while heat flux $\mathbf{q}$ has components

$$q_1 = -K_{11}\theta_{,1}, \qquad q_2 = -K_{22}\theta_{,2}, \qquad q_3 = 0. \tag{46}$$

If plane stress condition is considered, all fluxes in the x_3 direction have vanishing values

$$\sigma_{33} = \sigma_{13} = \sigma_{23} = 0, \qquad D_3 = 0, \qquad q_3 = 0.$$

In this second case, condensation of constitutive tensors leads to the following constitutive equations for the stress $\boldsymbol{\sigma}$, the electric displacement $\boldsymbol{D}$, and the heat flux $\boldsymbol{q}$ in the $\{x_1, x_2\}$ plane

$$
\begin{aligned}
\sigma_{11} &= \left[C_{1111} - \frac{C_{1133}(C_{1133}+e_{333}e_{113}/\beta_{33})}{C_{3333}+e_{333}^2/\beta_{33}} + \frac{e_{113}^2}{\beta_{33}} - \frac{e_{113}e_{333}(C_{1133}+e_{333}e_{113}/\beta_{33})}{\beta_{33}(C_{3333}+e_{333}^2/\beta_{33})}\right]\varepsilon_{11} \\
&+ \left[C_{1122} - C_{1133}\frac{C_{2233}+e_{223}e_{333}/\beta_{33}}{C_{3333}+e_{333}^2/\beta_{33}} + \frac{e_{113}e_{223}}{\beta_{33}} - \frac{e_{113}e_{333}(C_{2233}+e_{223}e_{333}/\beta_{33})}{\beta_{33}(C_{3333}+e_{333}^2/\beta_{33})}\right]\varepsilon_{22} \\
&- \left[\alpha_{11} - \frac{C_{1133}(\alpha_{33}-e_{333}\gamma_3/\beta_{33})}{C_{3333}+e_{333}^2/\beta_{33}} - \frac{e_{113}\gamma_3}{\beta_{33}} - \frac{e_{113}e_{333}(\alpha_{33}-e_{333}\gamma_3/\beta_{33})}{\beta_{33}(C_{3333}+e_{333}^2/\beta_{33})}\right]\theta, \\
\sigma_{22} &= \left[C_{2222} - \frac{C_{2233}(C_{2233}+e_{333}e_{223}/\beta_{33})}{C_{3333}+e_{333}^2/\beta_{33}} + \frac{e_{223}^2}{\beta_{33}} - \frac{e_{223}e_{333}(C_{2233}+e_{333}e_{223}/\beta_{33})}{\beta_{33}(C_{3333}+e_{333}^2/\beta_{33})}\right]\varepsilon_{22} \\
&+ \left[C_{2211} - C_{2233}\frac{C_{1133}+e_{113}e_{333}/\beta_{33}}{C_{3333}+e_{333}^2/\beta_{33}} + \frac{e_{223}e_{113}}{\beta_{33}} - \frac{e_{223}e_{333}(C_{1133}+e_{113}e_{333}/\beta_{33})}{\beta_{33}(C_{3333}+e_{333}^2/\beta_{33})}\right]\varepsilon_{11} \\
&- \left[\alpha_{22} - \frac{C_{2233}(\alpha_{33}-e_{333}\gamma_3/\beta_{33})}{C_{3333}+e_{333}^2/\beta_{33}} - \frac{e_{223}\gamma_3}{\beta_{33}} - \frac{e_{223}e_{333}(\alpha_{33}-e_{333}\gamma_3/\beta_{33})}{\beta_{33}(C_{3333}+e_{333}^2/\beta_{33})}\right]\theta, \\
\sigma_{12} &= 2C_{1212}\varepsilon_{12}, \qquad (47a) \\
D_1 &= -\left[\beta_{11} + \frac{e_{131}^2}{C_{1313}}\right]\phi_{,1} + \gamma_1\theta, \\
D_2 &= -\left[\beta_{22} + \frac{e_{233}^2}{C_{2323}}\right]\phi_{,2} + \gamma_2\theta, \qquad (47b) \\
q_1 &= -K_{11}\theta_{,1}, \\
q_2 &= -K_{22}\theta_{,2}. \qquad (47c)
\end{aligned}
$$

5.2 Homogenization of benders' microstructured layer: perturbation functions and overall constitutive tensors

Solution of cell problems (9), (12), (15), and (19) allows to derive perturbation functions relative to the order ε^{-1}. Fluctuation functions consider the influence of material inhomogeneities on the micro fields and on the coupling among them. They are exclusively dependent on the geometric and physico-mechanical features of the material at hand. One considers periodic cells $\mathcal{A}$ as the ones illustrated in figures 4, characterized respectively by a circular and a square inclusion. Figures 5 and 6 show some of the perturbation functions derived on the unit cell $\mathcal{Q}$ from a numerical resolution of cell problems (9), (12), (15), and (19) at the order ε^{-1} in plane strain conditions trough a finite element discretization. To this aim periodicity conditions have been imposed for all the perturbation functions over $\mathcal{Q}$. To this purpose an ad hoc thermo-piezolectric finite element has been implemented in the finite element software FEAP. Interested readers can find details regarding the formulation of such thermo-piezoelectric finite element framework in Appendix C of (Fantoni et al., 2017). Illustrated perturbation functions refer to the case of a volume fraction $f = 0.25$ for both the circular inclusion (figure 5), and the square one (figure 6), where f is defined as the ratio between the area of the inclusion and the area of the periodic cell. It is evident from figures 5 and 6 that perturbation functions have vanishing mean values over $\mathcal{Q}$ by virtue of the imposed normalization condition (8).

Closed form expressions (32) and (36) allow to compute the overall constitutive tensors for the first-order homogenized continuum for the plane stress and plane strain conditions described above. For example, at $f = 0.25$ and for circular inclusion, indicated by apex ^{circ}, overall constitutive tensors have the following expression in plane strain conditions

$$
\mathbb{C}^{circ} = \begin{pmatrix} 2.45 & 1.80 & 0 \\ 1.80 & 2.45 & 0 \\ 0 & 0 & 2\cdot 0.30 \end{pmatrix} 10^9 \frac{\mathrm{N}}{\mathrm{m}^2}, \quad \boldsymbol{\beta}^{circ} = \begin{pmatrix} 0.61 & 0 \\ 0 & 0.61 \end{pmatrix} 10^{-9} \frac{\mathrm{C}}{\mathrm{V\,m}},
$$

$$
\boldsymbol{K}^{circ} = \begin{pmatrix} 0.57 & 0 \\ 0 & 0.57 \end{pmatrix} \frac{\mathrm{W}}{\mathrm{m\,K}}, \quad \boldsymbol{\alpha}^{circ} = \begin{pmatrix} 1.67 \\ 1.67 \\ 0 \end{pmatrix} 10^5 \frac{\mathrm{N}}{\mathrm{m^2\,K}},
$$

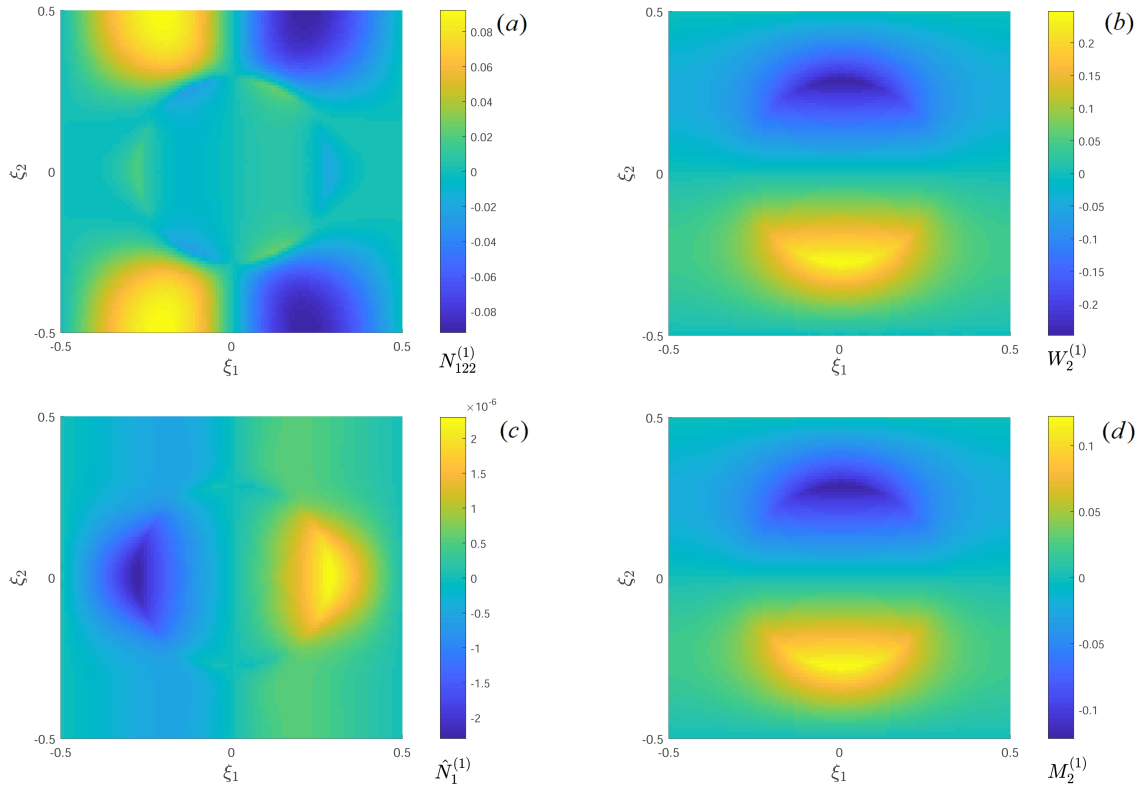

Figure 5: *Some of the perturbation functions obtained by means of numerical resolution of cell problems at the order ε^{-1} over the unit cell $\mathcal{Q}$ with circular inclusion and $f = 0.25$: (a) $N^{(1)}_{122}$, (b) $W^{(1)}_2$, (c) $\hat{N}^{(1)}_1$, (d) $M^{(1)}_2$*

$$\boldsymbol{\gamma}^{circ} = \begin{pmatrix} 0.19 \\ 0.19 \end{pmatrix} 10^{-4} \frac{\mathrm{C}}{\mathrm{m^2\,K}}, \tag{48}$$

Considering a square inclusion, indicated by apex ^{sq}, at the same volume fraction $f = 0.25$ and plane strain conditions, overall constitutive tensors result

$$\mathbb{C}^{sq} = \begin{pmatrix} 5.53 & 2.96 & 0 \\ 2.96 & 5.53 & 0 \\ 0 & 0 & 2 \cdot 0.86 \end{pmatrix} 10^{8} \frac{\mathrm{N}}{\mathrm{m^2}}, \quad \boldsymbol{\beta}^{sq} = \begin{pmatrix} 0.35 & 0 \\ 0 & 0.35 \end{pmatrix} 10^{-10} \frac{\mathrm{C}}{\mathrm{V\,m}},$$

$$\boldsymbol{K}^{sq} = \begin{pmatrix} 0.56 & 0 \\ 0 & 0.56 \end{pmatrix} \frac{\mathrm{W}}{\mathrm{m\,K}}, \quad \boldsymbol{\alpha}^{sq} = \begin{pmatrix} 1.05 \\ 1.05 \\ 0 \end{pmatrix} 10^{5} \frac{\mathrm{N}}{\mathrm{m^2\,K}},$$

$$\boldsymbol{\gamma}^{sq} = \begin{pmatrix} 0.49 \\ 0.49 \end{pmatrix} 10^{-6} \frac{\mathrm{C}}{\mathrm{m^2\,K}}, \tag{49}$$

Figures 7 and 8 show the components of the overall constitutive tensors with respect to volume fraction f for the case of circular and square inclusion, considering plane strain and plane stress conditions. In particular, figures 7 and 8 represent the dimensionless components of the overall tensors, obtained dividing each component of the tensors by the averaged value of the same component relative to the inclusion computed for the plane stress and the plane strain cases. Indicating with $\boldsymbol{B}$ the generic overall tensor, dimensionless overall tensors are therefore defined as:

$$\hat{\boldsymbol{B}} = \frac{2\,\boldsymbol{B}}{\boldsymbol{B}_{PZT|_{x_3\,pl.strain}} + \boldsymbol{B}_{PZT|_{x_3\,pl.stress}}}$$

Figure 7 shows the non vanishing components of the overall constitutive tensors for the case of a circular inclusion whose radius increases monotonically such that $0 \leq f \leq 0.75$.

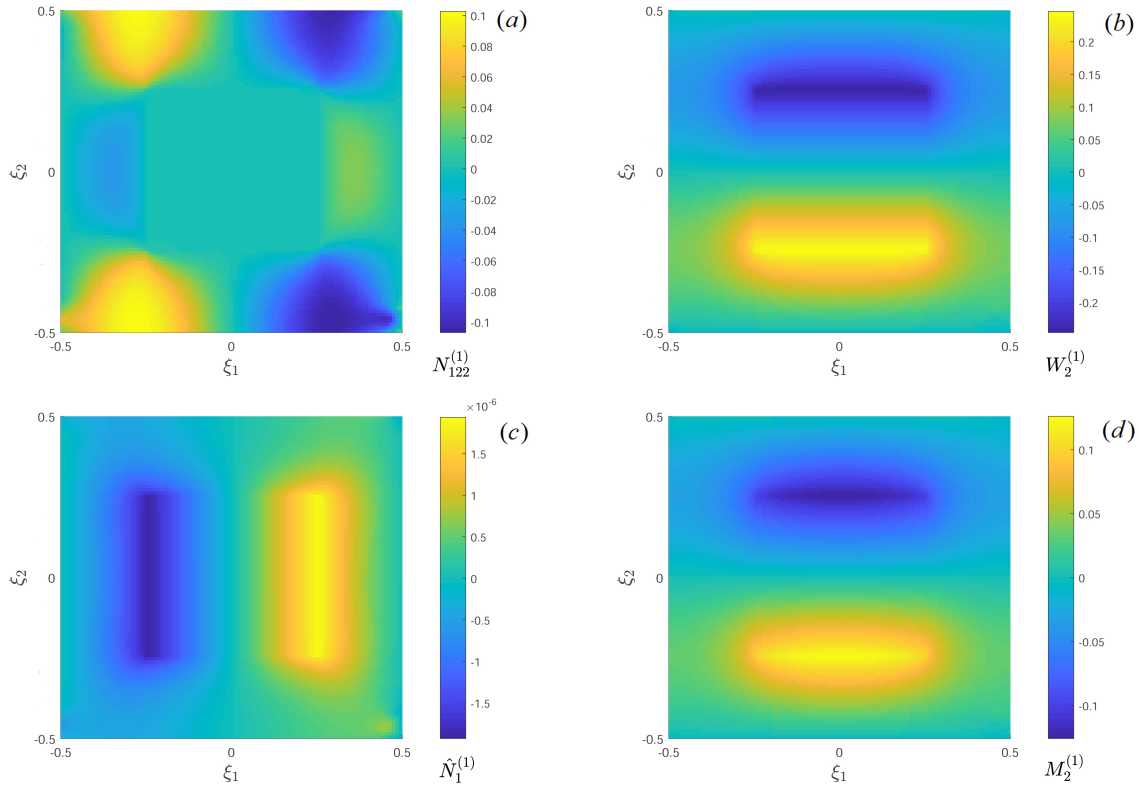

Figure 6: *Some of the perturbation functions obtained by means of numerical resolution of cell problems at the order ε^{-1} over the unit cell $\mathcal{Q}$ with square inclusion and $f = 0.25$: (a) $N^{(1)}_{122}$, (b) $W^{(1)}_2$, (c) $\hat{N}^{(1)}_1$, (d) $M^{(1)}_2$*

As shown in figure 7, computed components for the plane strain case are greater than the corresponding ones computed for the plane stress situation for all the overall tensors except in the case of the overall permittivity tensor $\boldsymbol{\beta}$. Figure 8 shows the non vanishing components of the overall constitutive tensors with respect to f for the case of a square inclusion increasing homotetically such that $0 \leq f \leq 0.25$. For values of volume fraction greater than 0.25 a rectangular inclusion has been considered, such that the length along the x_2 axis is kept fixed and equal to $0.5\,\varepsilon$, while the length along the x_1 axis increases such that $0.25 < f \leq 0.4$. As shown in figure 8, values for the plane strain situation are distinct and greater than the corresponding ones relative to the plane stress case for tensors $\mathbb{C}$, $\boldsymbol{\alpha}$, and $\boldsymbol{\gamma}$. Furthermore it is evident that, for $f > 0.25$, overall tensors stop to be isotropic, diversifying the behavior along the x_1 and x_2 axes.

5.3 Unimorph and bimorph bender actuators

Deflection of unimorph and bimorph benders as the ones illustrated in figure 3 has been studied in plane strain conditions varying the volume fraction f of the PZT inclusions in the composite layer, considering in this stratum the presence of circular and square/rectangular PZT fibers (see figure 4). Benders are considered fixed at one end trough translational constraints. One defines the following dimensionless quantities:

$$x_1^* = \frac{x_1}{L}, \quad x_2^* = \frac{x_2}{H}, \quad U_1^* = \frac{U_1}{L}, \quad U_2^* = \frac{U_2}{L}, \quad \Phi^* = \frac{\Phi\sqrt{\beta_{11_{PZT|x_3}}}}{\sqrt{C_{1111_{PZT|x_3}}}\,L}, \quad \Theta^* = \frac{\Theta\alpha_{11_{PZT|x_3}}}{C_{11_{PZT|x_3}}}. \tag{50}$$

where L and H are the overall length and height of benders respectively, as depicted in figure 3. Resolution of the coupled thermo-electro-mechanical problem has been achieved by means of finite element analyses of bender actuators with the software FEAP, modeling the presence of two (unimorph) or three (bimorph) layers. Details of the formulation and implementation of the adopted thermo-piezoelectric finite element

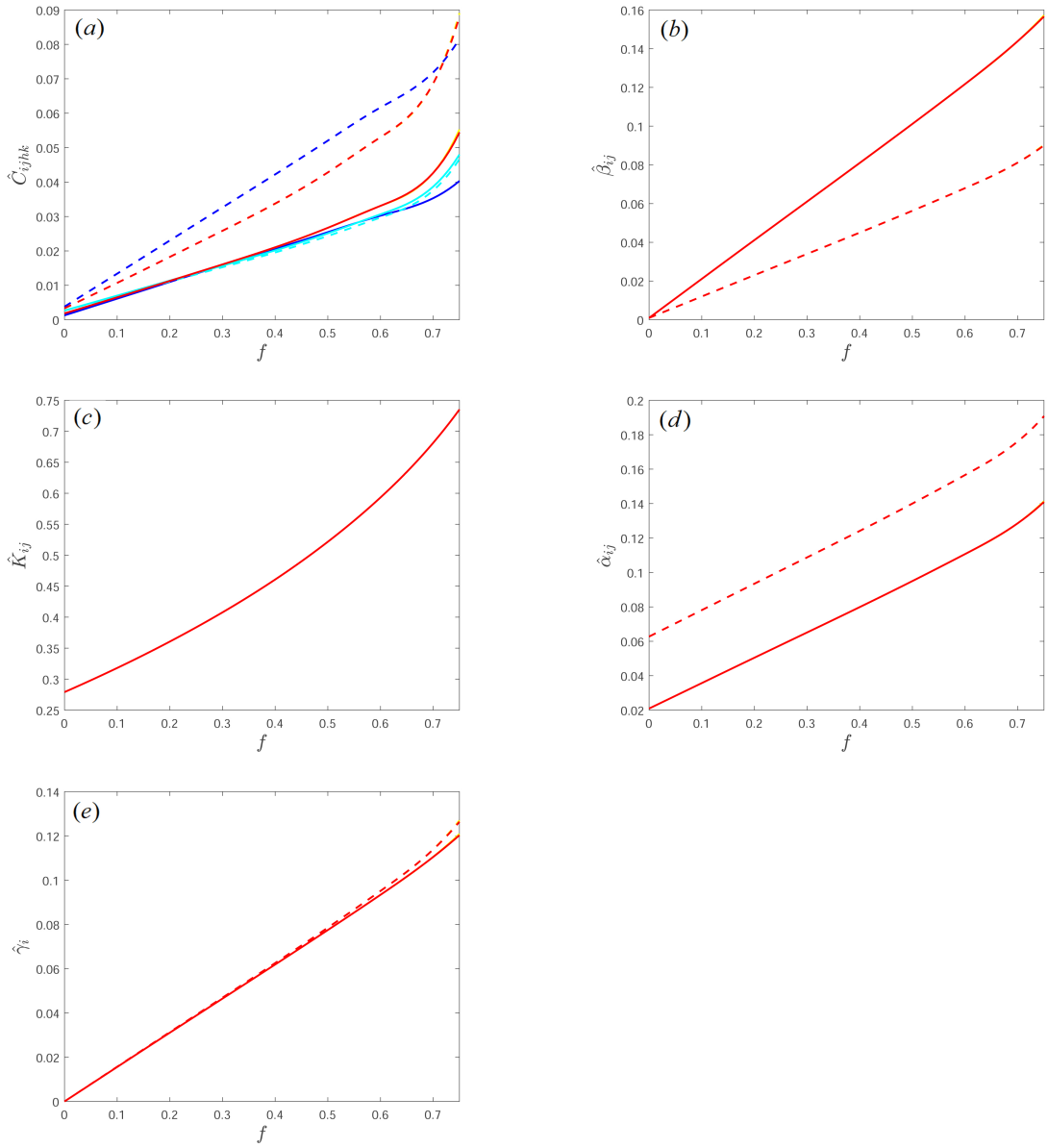

Figure 7: *Dimensionless components of the overall constitutive tensors vs volume fraction* f*, with* $0 \leq f \leq 0.75$ *and circular inclusion for plane stress (continuous line) and plane strain (dashed line) conditions. (a)* $\hat{C}_{1111} = \hat{C}_{2222}$ *(red curve),* $\hat{C}_{1122}$ *(blue curve),* $\hat{C}_{1212}$ *(light blue curve), (b)* $\hat{\beta}_{11} = \hat{\beta}_{22}$*, (c)* $\hat{K}_{11} = \hat{K}_{22}$*, (d)* $\hat{\alpha}_{11} = \hat{\alpha}_{22}$*, (e)* $\hat{\gamma}_1 = \hat{\gamma}_2$

procedure can be found in Appendix C of (Fantoni et al., 2017). Figure 9 shows the deflection of the benders with respect to volume fraction f, for three different values of the benders slenderness, namely $H/L = 1/10, 1/20, 1/40$ and a ratio between the thickness of the composite layer and the PZT one equal to $h_c/h_P = 2$. Benders are loaded applying a voltage equal to $\Delta\Phi^* = 5.8 \cdot 10^{(-7)}$ between electrodes, as indicated in figure 3. In particular, dimensionless values of the macro displacement $\tilde{U}_2$ are represented in figure 9, this last defined as the ratio between displacement U_2 measured at the free end of benders with coordinates $x_1 = L$ and $x_2 = 0$ and the corresponding value obtained at the same point for $f = 0$, namely $\tilde{U}_2 = U_{2|f}/U_{2|f=0}$. As shown in figures 9-(a) and 9-(c) the deflection of the unimorph bender is not influenced by the slenderness, increasing monotonically as f raises, reaching a maximum value equal to 6.6 for circular inclusion and equal to 3.2 for square inclusion. On the contrary, the behavior of the bimorph bender is

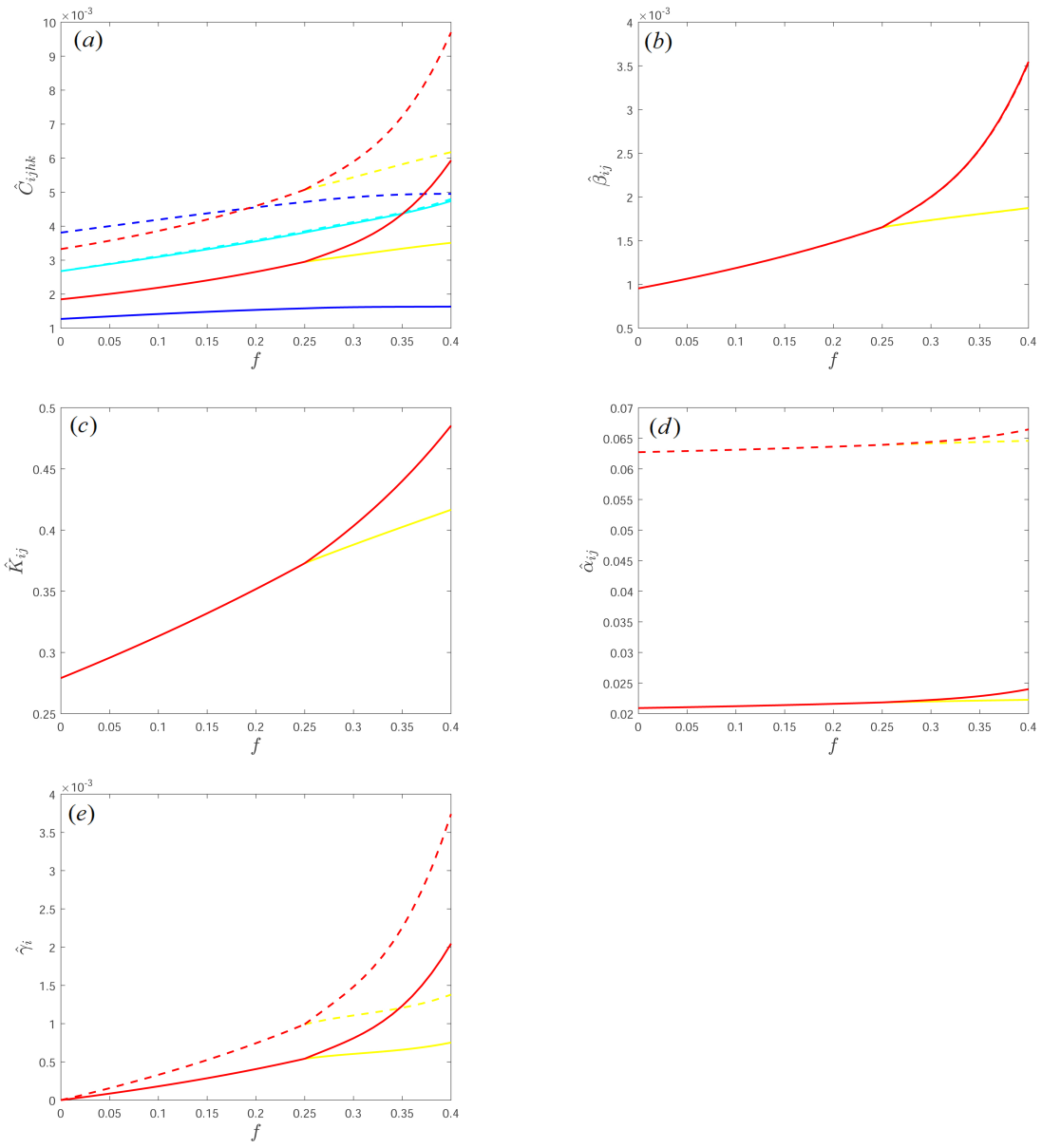

Figure 8: *Dimensionless components of the overall constitutive tensors vs volume fraction* f*, with* $0 \leq f \leq 0.4$ *and square/rectangular inclusion for plane stress (continuous line) and plane strain (dashed line) conditions. (a)* $\hat{C}_{1111}$ *(red curve),* $\hat{C}_{2222}$ *(yellow curve),* $\hat{C}_{1122}$ *(blue curve),* $\hat{C}_{1212}$ *(light blue curve), (b)* $\hat{\beta}_{11}$ *(red curve),* $\hat{\beta}_{22}$ *(yellow curve), (c)* $\hat{K}_{11}$ *(red curve),* $\hat{K}_{22}$ *(yellow curve), (d)* $\hat{\alpha}_{11}$ *(red curve),* $\hat{\alpha}_{22}$ *(yellow curve), (e)* $\hat{\gamma}_1$ *(red curve),* $\hat{\gamma}_2$ *(yellow curve)*

strongly influenced by the slenderness, increasing the deflection as the ratio H/L increases. For the case of the circular inclusion, values of $\tilde{U}_2$ reach their maximum at $f = 0.5$ for each value of the ratio H/L and, in particular, for $H/L = 1/40$, the dimensionless displacement $\tilde{U}_2$ becomes less than 1 for $f > 0.5$, meaning that the presence of the PZT fibers in the composite layer lowers the bender deflection with respect to the case without fibers. For the square inclusion case, deflection of the bimorph bender increases monotonically as f increases for $H/L = 1/10$ and $H/L = 1/20$, while reaches its maximum at $f = 0.3$ and decreases for $f > 0.3$ in the case $H/L = 1/40$. Except for the case of bimorph bender and H/L=1/40, values of $\tilde{U}_2$ for circular inclusions are greater than the corresponding ones for square inclusions at the same value of volume fraction f, meaning that fibers topology plays a role in characterizing the behavior of the actuator. Furthermore,

in all cases here analyzed, values of $\tilde{U}_2$ for the bimorph bender are lower than the unimorph bender ones. This means that the presence of a microstructured composite layer influences the stiffness of the unimorph bender more than it does for the bimorph one.
Figure 10 shows the deflection of the unimorph and bimorph benders with respect to f for $H/L = 1/20$ and three different values of the ratio between the thickness of the composite layer and the PZT one, namely $h_c/h_P = 2, 1, 1/2$. As shown in figure 10 values of $\tilde{U}2$ are greatly influenced by the parameter h_c/h_P, increasing as h_c/h_P decreases. Values of dimensionless displacement $\tilde{U}_2$ increase monotonically in all cases except for the case of bimorph bender with circular inclusion and $h_c/h_P = 1$ and $h_c/h_P = 2$ for which $\tilde{U}_2$ reaches its maximum at $f = 0.6$. Once again, values of $\tilde{U}_2$ for the circular inclusion cases are greater than the corresponding ones for square inclusion at the same f and $\tilde{U}_2$ values for the unimorph bender are greater than the ones relative to the bimorph bender, reaching values almost equal to 30 for the case of unimorph bender with circular inclusion and $h_c/h_P = 1/2$.

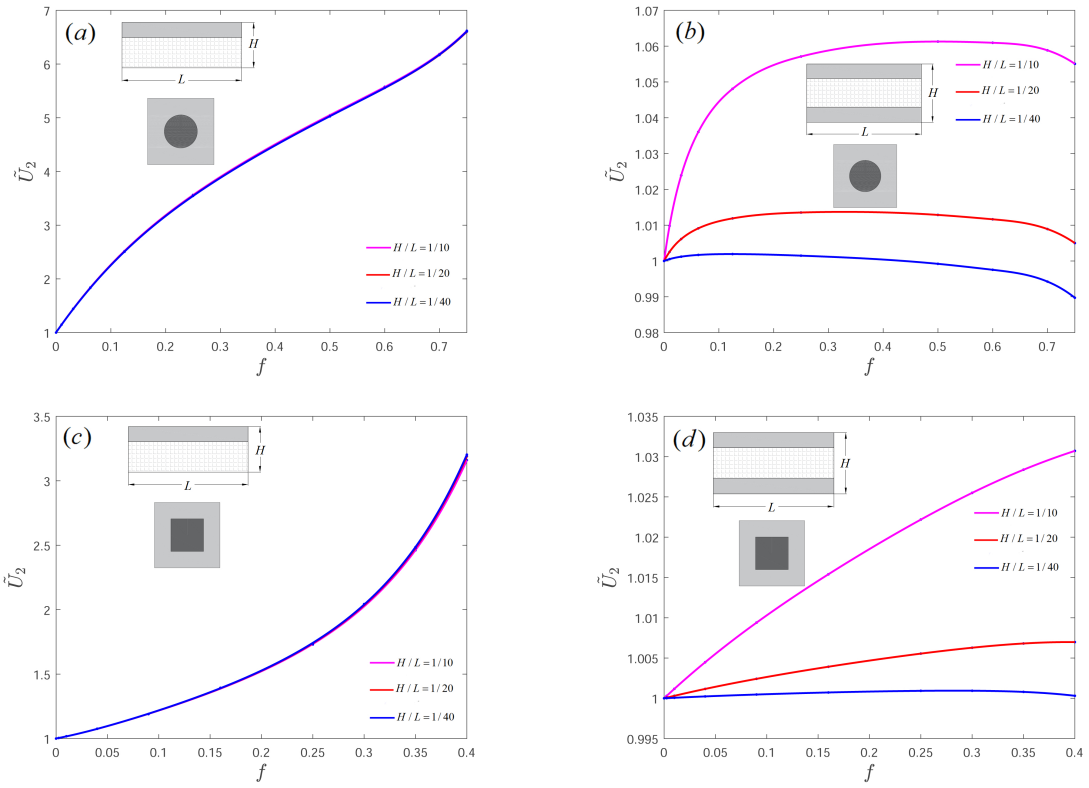

Figure 9: *Dimensionless macro displacement $\tilde{U}_2$ vs volume fraction f for $h_c/h_P = 2$ and three different values of bender slenderness. Each figure contains a sketch of the bender and inclusion topology to which it refers.*

Furthermore, in order to analyze the influence of the pyroelectric properties of the material on the global behavior of the bender, deflection of unimorph and bimorph benders has been studied by applying, in addition to voltage $\Delta\Phi^*$, a relative temperature gradient between the upper and lowers edges of the actuators equal to $\Delta\Theta^* = \Theta^*_{ext} - \Theta^*_{int}$ (see figure 3). Figure 11 shows the dimensionless displacement $\tilde{U}_2$ at the free end of the benders with respect to volume fraction f for five different values of the ratio $\eta = \Delta\Phi^*/\Delta\Theta^*$, namely $\eta = 1/10, 1/5, 1, 5, 10$.

As shown in figure 11, $\tilde{U}_2$ increases as η increases. For values of $\eta \leq 1$, deflection of the benders greatly depends on η, while this doesn't happen when $\eta > 1$. In fact, obtained curves for $\eta = 5$ and $\eta = 10$ are almost overlapped for all the cases represented in figure 11. Dimensionless displacement $\tilde{U}_2$ increases monotonically with f, except for the case of bimorph bender and circular inclusion represented in figure 11-(b). Furthermore, for the case of unimorph bender and circular inclusion, the heterogeneity of the material at the macroscale is responsible of the presence of surface forces which act at the interface between the homogenized composite

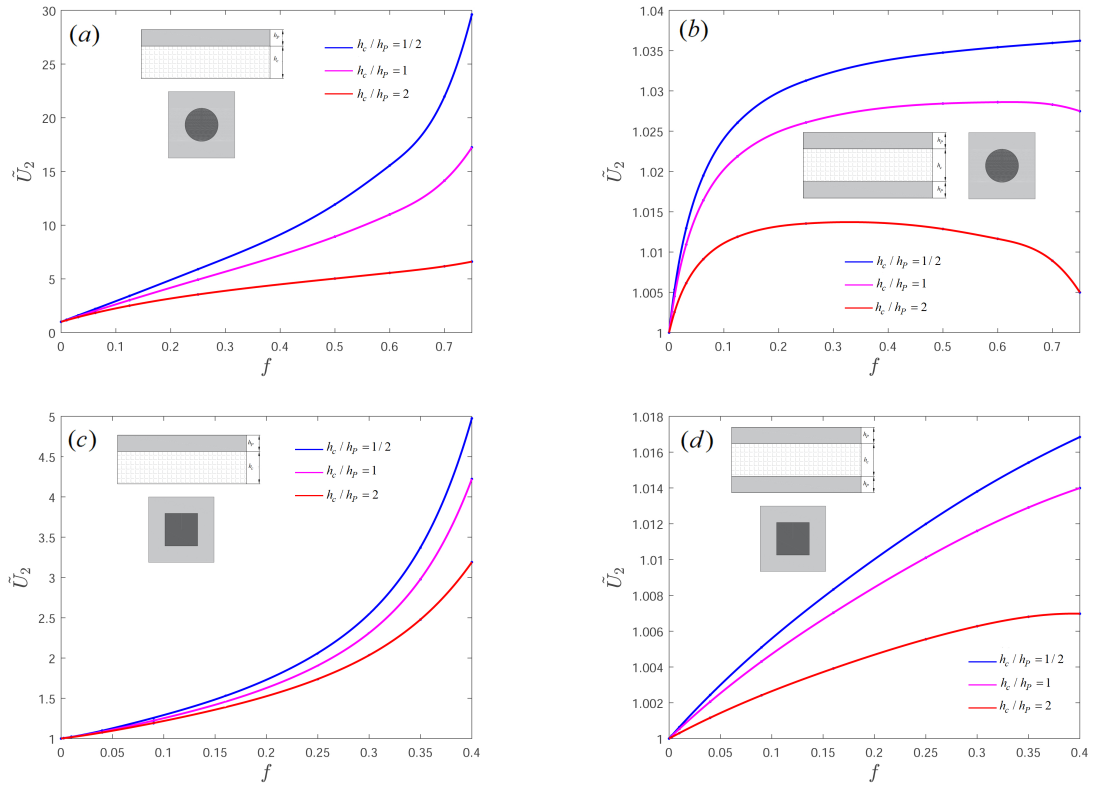

Figure 10: *Dimensionless macro displacement $\tilde{U}_2$ vs volume fraction f for $H/L = 1/20$ and three different values of h_c/h_P. Each figure contains a sketch of the bender and inclusion topology to which it refers.*

layer and the PZT one whose values are such that the bender manifests a non intuitive behavior for $f \leq 0.125$ when subject to $\Delta\Theta^*$. Such surface forces are generated by the mismatch that exists between the components of the elastic tensor $\mathbb{C}_{PZT|x_2}$ and of the thermal dilatation tensor $\boldsymbol{\alpha}_{PZT|x_2}$ relative to the PZT layer and the corresponding ones of the homogenized composite layer. Namely, if $\Theta^*_{ext} > \Theta^*_{int}$, the bender deflects upward if $f \leq 0.125$, contrarily to what would happen if the material was homogeneous. If one considers the not normalized macro displacement U_2, it is evident that at $f = 0.125$ there is an inversion of tendency of U_2 curves with respect to η.
Finally, figures 12 and 13 show the contour plots of the dimensionless macro fields U_1^*, U_2^*, Φ^* and Θ^*, as expressed in equation (50), for one of the analyzed load cases, namely $\eta = 1$, $H/L = 1/20$, $h_c/h_P = 2$, circular inclusion and $f = 1/4$ for the unimorph and bimorph benders.

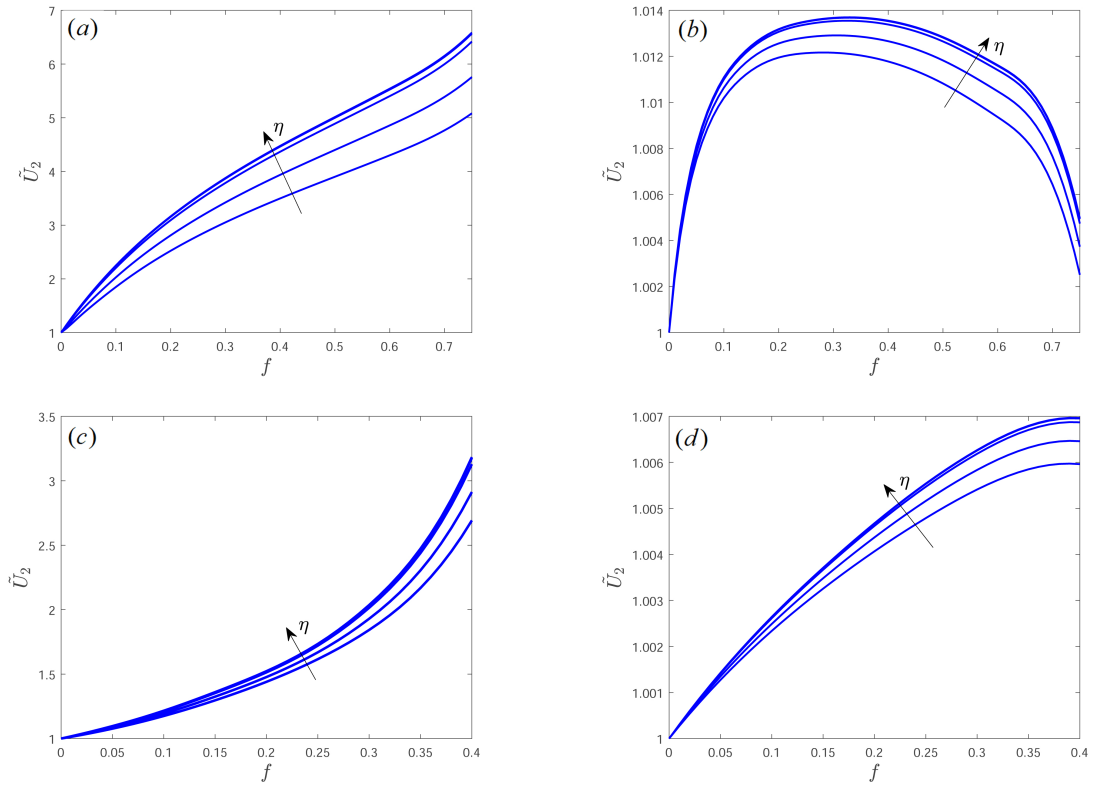

Figure 11: *Dimensionless macro displacement* $\tilde{U}_2$ *vs volume fraction* f *for five different values of* $\eta = \Delta\Phi^*/\Delta\Theta^*$, *namely* $\eta = 1/10, 1/5, 1, 5, 10$.*Arrows in the graphs indicate the direction of increasing* η. *(a) Unimorph bender and circular inclusion, (b) bymorph bender and circular inclusion, (c) unimorph bender and square/rectangular inclusion, (d) bimorph bender and square/rectangular inclusion.*

6 Conclusions

Applications of piezoelectric and pyroelectric devices are several, especially as sensing and actuating means. High precision required in the manufacturing process, remarkably in the case of MEMS, leads to the need of accurate preliminary computations. In this regard, determination of proper constitutive relations characterizing the medium at the macroscale could reveal of great importance in order to optimize the performance of the device. The multi-field asymptotic homogenization model obtained in (Fantoni et al., 2017) is here presented as it constitutes a rigorous tool for the characterization of thermo-piezoelectric materials with periodic microstructure, avoiding the challenging computational need to model the whole heterogeneous structure. Down-scaling relations are provided; they associate the microscopic displacement, electric potential and relative temperature to the corresponding macroscopic fields and their coupling by means of perturbation functions. These lasts are obtained trough the resolution of non homogeneous recursive cell problems over the unit cell $\mathcal{Q}$. Such functions reflect the effect of the microstructural heterogeneity on the micro fields and on the coupling between them. They result to be $\mathcal{Q}$-periodic, with a vanishing mean value over $\mathcal{Q}$ for the imposed normalization condition. Field equations of the homogenized first-order (Cauchy) medium equivalent to the heterogeneous thermo-piezoelectric one have been determined truncating at the zeroth order the average field equations of infinite order asymptotically expanded in powers of the microstructural size in terms of the macroscopic fields. Exact expressions of the overall constitutive tensors have been determined for the equivalent first-order homogenized material. The accuracy of the obtained multi-field first-order asymptotic homogenization technique has been assessed in (Fantoni et al., 2017), where the good agreement obtained between the homogenized solution and the numerical one relative to the heterogeneous model subject to harmonic volume forces confirms the validity of the proposed method.
In the present study unimorph and bimorph pyroelectric bending actuators are analyzed in plane stress and

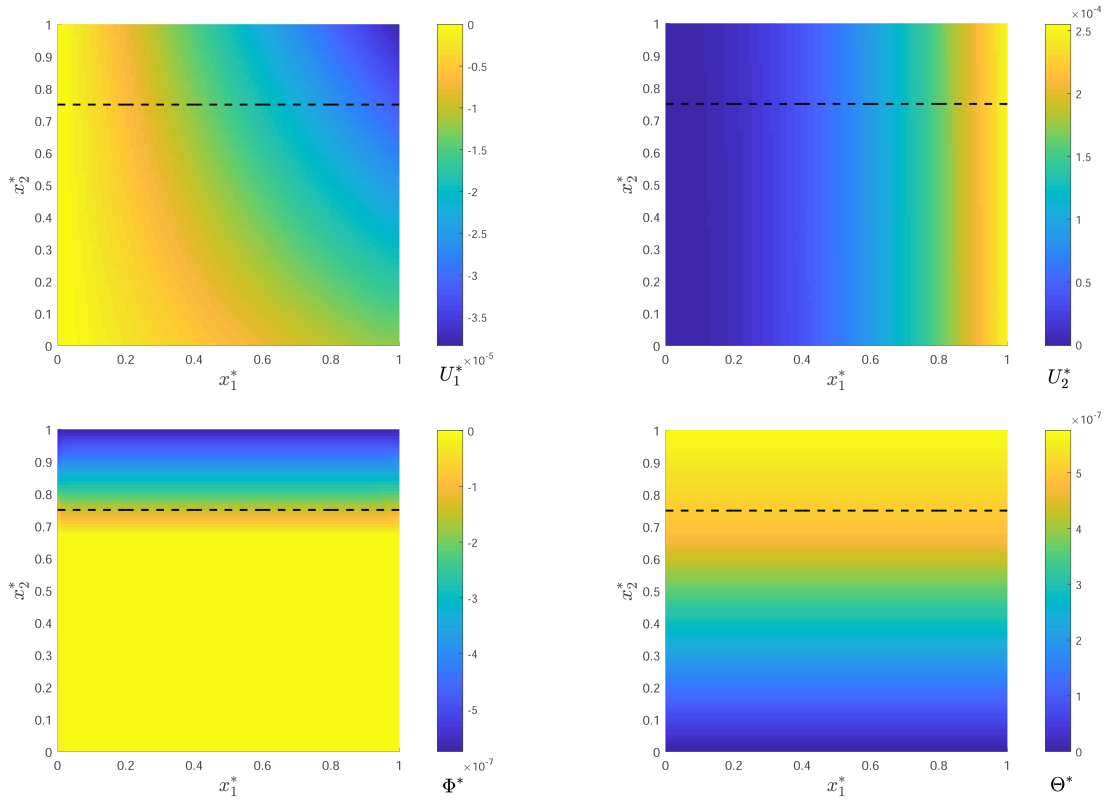

Figure 12: *Contour plots of the macro fields relative to the unimorph bender with circular fibers and* $f = 1/4$ *subject to* $\Delta\Phi^*$ *and* $\Delta\Theta^*$ *such that* $\eta = \Delta\Phi^*/\Delta\Theta^* = 1$. *Black dashed line indicates the interface between the PZT layer and the composite one. (a)* U_1^*, *(b)* U_2^*, *(c)* Φ^*, *(d)* Θ^*.

plane strain conditions. They consist of active laminae made of PZT with an in plane polarization and a microstructured composite layer with periodic microstructure where PZT fibers, polarized in the out of plane direction, are immersed in a polymeric passive matrix. The previously described multi-field asymptotic technique, developed for thermo-piezoelectric materials, has been exploited to derive the constitutive law of the composite layer at the mesoscale, considering different topologies of the PZT inclusions. Deflection of benders has been investigated in relation to some geometrical features in order to study the influence of the microstructure on the overall stiffness of the actuator. From the analyzed cases it resulted that in the case of composite layer with circular inclusions the benders, loaded by an imposed voltage and/or relative temperature gradient, deflect more than for the case of square/rectangular fibers at the same values of inclusion volume fraction, both for the unimorph and bimorph cases. Circular inclusions are therefore preferable to square ones in order to increase device performances. Furthermore, in all the investigated cases unimorph benders deflect more than bimorph devices do for the same inclusion topology and at the same values of volume fraction of the inclusions, meaning that the presence of a microstructured composite layer influences the stiffness of the unimorph actuators more than it does for the bimorph devices. In particular, in the presence of a microstructured composite layer unimorph benders increase their performance much more than the bimorph counterparts do with respect to the case of a passive layer without pyroelectric inclusions. Concluding, the evaluation of the overall thermo-piezoelectric properties of pyroelectric devices through the multi-field asymptotic homogenization approach illustrated in the paper can represent an important issue in order to improve the efficient design and manufacturing of such systems. Proposed first-order asymptotic homogenization model can be extended to higher orders to properly describe non local phenomena or, equivalently, high gradients of stresses, deformations, electric potential, relative temperature, and volume forces. Alternatively, in order to derive constitutive relations of equivalent higher order continua, nonlocal higher order homogenization techniques involving characteristic length scale associated to the microstructural effects, can be conveniently deployed, but these topics are out of the scope of the present note.

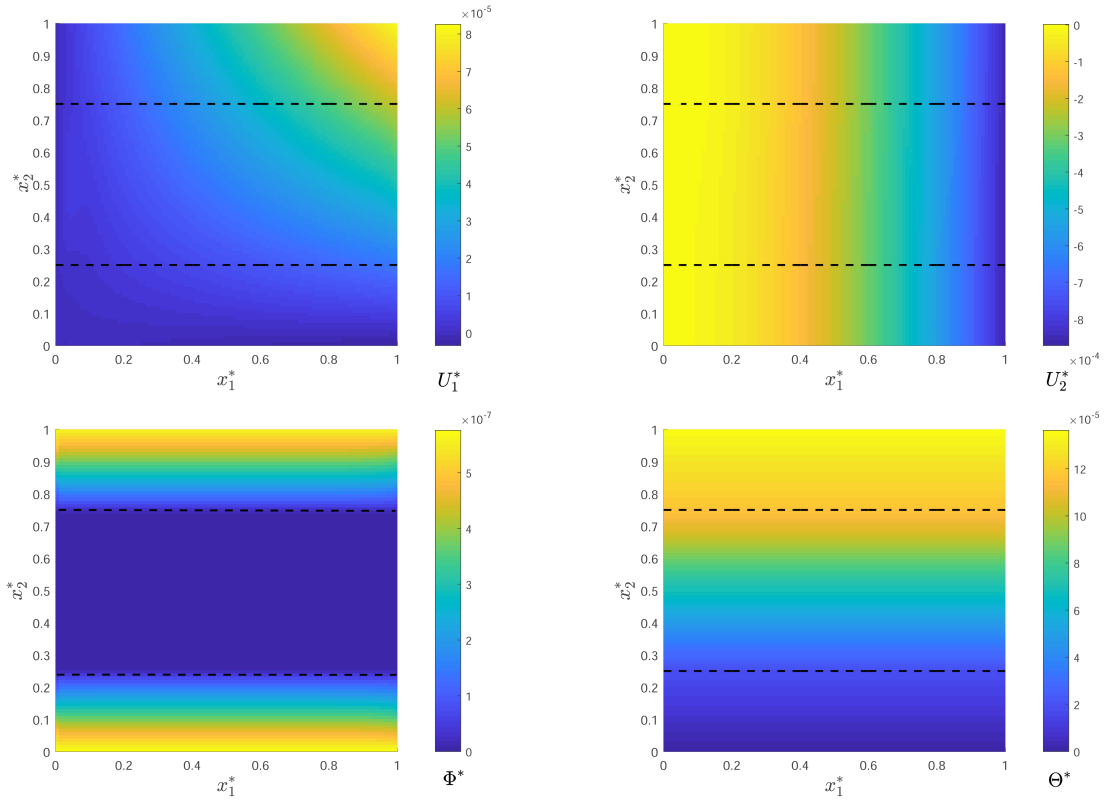

Figure 13: *Contour plots of the macro fields relative to the bimorph bender with circular fibers and* $f = 1/4$ *subject to* $\Delta\Phi^*$ *and* $\Delta\Theta^*$ *such that* $\eta = \Delta\Phi^*/\Delta\Theta^* = 1$. *Black dashed lines indicate the interfaces between the PZT layers and the composite one. (a)* U_1^*, *(b)* U_2^*, *(c)* Φ^*, *(d)* Θ^*.

References

Addessi, D., De Bellis, M., Sacco, E., 2013. Micromechanical analysis of heterogeneous materials subjected to overall cosserat strains. Mechanics Research Communications 54, 27–34.

Addessi, D., De Bellis, M. L., Sacco, E., 2016. A micromechanical approach for the cosserat modeling of composites. Meccanica 51 (3), 569–592.

Anton, S. R., Sodano, H. A., 2007. A review of power harvesting using piezoelectric materials (2003–2006). Smart materials and Structures 16 (3), R1.

Bacca, M., Bigoni, D., Dal Corso, F., Veber, D., 2013a. Mindlin second-gradient elastic properties from dilute two-phase cauchy-elastic composites. part i: Closed form expression for the effective higher-order constitutive tensor. International Journal of Solids and Structures 50(24), 4010–4019.

Bacca, M., Bigoni, D., Dal Corso, F., Veber, D., 2013b. Mindlin second-gradient elastic properties from dilute two-phase cauchy-elastic composites part ii: Higher-order constitutive properties and application cases. international journal of solids and structures. International Journal of Solids and Structures 50(24), 4020–4029.

Bacca, M., Dal Corso, F., Veber, D., Bigoni, D., 2013c. Anisotropic effective higher-order response of heterogeneous cauchy elastic materials. Mechanics Research Communications 54, 63–71.

Bacigalupo, A., 2014. Second-order homogenization of periodic materials based on asymptotic approximation of the strain energy: formulation and validity limits. Meccanica 49(6), 1407–1425.

Bacigalupo, A., Gambarotta, L., 2014. Computational dynamic homogenization for the analysis of dispersive waves in layered rock masses with periodic fractures. Computers and Geotechnics 56, 61–68.

Bacigalupo, A., Morini, L., Piccolroaz, A., 2014. Effective elastic properties of planar sofcs: A non-local dynamic homogenization approach. International Journal of Hydrogen Energy 39(27), 15017–15030.

Bacigalupo, A., Morini, L., Piccolroaz, A., 2016a. Multiscale asymptotic homogenization analysis of thermo-diffusive composite materials. International Journal of Solids and Structures 85-86, 15–33.

Bacigalupo, A., Morini, L., Piccolroaz, A., 2016b. Overall thermomechanical properties of layered materials for energy devices applications. Composite Structures 157, 366–385.

Bacigalupo, A., Paggi, M., Dal Corso, F., Bigoni, D., 2017. Identification of higher-order continua equivalent to a cauchy elastic composite. Mechanics Research Communications, http://dx.doi.org/10.1016/j.mechrescom.2017.07.002.

Bakhvalov, N., Panasenko, G., 1984. Homogenization: Averaging Processes in Periodic Media. Kluwer Academic Publishers, Dordrecht-Boston-London.

Batra, A., Aggarwal, M., 2013. Pyroelectric Materials: Infrared Detectors, Particle Accelerators and Energy Harvesters. SPIE Press.

Bensoussan, A., Lions, J., Papanicolaou, G., 1978. Asymptotic analysis for periodic structures. North-Holland, Amsterdam.

Bigoni, D., Drugan, W., 2007. Analytical derivation of cosserat moduli via homogenization of heterogeneous elastic materials. Journal of Applied Mechanics 74(4), 741–753.

Brand, O., Fedder, G. K., Hierold, C., Korvink, J. G., Tabata, O., 2015. Micro energy harvesting. John Wiley & Sons.

Bravo-Castillero, J., Rodríguez-Ramos, R., Mechkour, H., Otero, J. A., Cabanas, J. H., Sixto, L., Guinovart-Díaz, R., Sabina, F. J., 2009. Homogenization and effective properties of periodic thermomagnetoelectroelastic composites. Journal of mechanics of materials and structures 4 (5), 819–836.

Cheng, H.-M., Ewe, M. T., Chiu, G. T., Bashir, R., 2001. Modeling and control of piezoelectric cantilever beam micro-mirror and micro-laser arrays to reduce image banding in electrophotographic processes. Journal of Micromechanics and Microengineering 11 (5), 487.

De Bellis, M. L., Bacigalupo, A., 2017. Auxetic behavior and acoustic properties of microstructured piezoelectric strain sensors. Smart Materials and Structures 26 (8), 085037.

De Lit, P., Agnus, J., Chaillet, N., 2003. The constitutive equations of a piezoelectric duo-bimorph. In: Assembly and Task Planning, 2003. Proceedings of the IEEE International Symposium on. IEEE, pp. 1–6.

Dunsch, R., Breguet, J.-M., 2007. Unified mechanical approach to piezoelectric bender modeling. Sensors and Actuators A: physical 134 (2), 436–446.

Fantoni, F., Bacigalupo, A., Paggi, M., 2017. Multi-field asymptotic homogenization of thermo-piezoelectric materials with periodic microstructure. International Journal of Solids and Structures 120, 31–56.

Forest, S., Sab, K., 1998. Cosserat overall modeling of heterogeneous materials. Mechanics Research Communications 25(4), 449–454.

Forest, S., Trinh, D., 2011. Generalized continua and nonhomogeneous boundary conditions in homogenisation methods. ZAMMJournal of Applied Mathematics and Mechanics/Zeitschrift fr Angewandte Mathematik und Mechanik 91(2), 90–109.

Galka, A., Telega, J., Wojnar, R., 1992. Homogenization and thermopiezoelectricity. Mechanics Research Communications 19 (4), 315–324.

Galka, A., Telega, J., Wojnar, R., 1996. Some computational aspects of homogenization of thermopiezoelectric composites. Comput. Assist. Mech. Eng. Sci 3 (2), 133–154.

Gardner, J. W., Varadan, V. K., Awadelkarim, O. O., 2001. Microsensors, MEMS, and smart devices. Vol. 1. Wiley Online Library.

Guo, Q., Cao, G., Shen, I., 2003. Measurements of piezoelectric coefficient d33 of lead zirconate titanate thin films using a mini force hammer. Journal of Vibration and Acoustics 135(1), 011003.

Hagood, N. W., von Flotow, A., 1991. Damping of structural vibrations with piezoelectric materials and passive electrical networks. Journal of Sound and Vibration 146 (2), 243–268.

Heinonen, E., Juuti, J., Jantunen, H., 2007. Characteristics of piezoelectric cantilevers embedded in ltcc. Journal of the European Ceramic Society 27 (13-15), 4135–4138.

Kang, Z., Wang, X., 2010. Topology optimization of bending actuators with multilayer piezoelectric material. Smart Materials and Structures 19 (7), 075018.

Kim, H. S., Kim, J.-H., Kim, J., 2011. A review of piezoelectric energy harvesting based on vibration. International journal of precision engineering and manufacturing 12 (6), 1129–1141.

Kommepalli, H., Mateti, K., Rahn, C., Tadigadapa, S., 2010. Displacement and blocking force performance of piezoelectric t-beam actuators. In ASME 2010 International Design Engineering Technical Conferences and Computers and Information in Engineering Conference American Society of Mechanical Engineers, 841–850.

Kouznetsova, V., Geers, M., Brekelmans, W., 2004. Multi-scale second-order computational homogenization of multi-phase materials: a nested finite element solution strategy. Computer Methods in Applied Mechanics and Engineering 193(48), 5525–5550.

Malmonge, L., Malmonge, J., Sakamoto, W., 2003. Study of pyroelectric activity of pzt/pvdf-hfp composite. Materials Research 6.4, 469–473.

Mehrabadi, M., Cowin, S., 1990. Eigentensors of linear anisotropic elastic materials. The Quarterly Journal of Mechanics and Applied Mathematics 43(1), 15–41.

Miehe, C., Schroder, J., Schotte, J., 1999. Computational homogenization analysis in finite plasticity simulation of texture development in polycrystalline materials. Computer methods in applied mechanics and engineering 171, 387–418.

Mindlin, R., 1974. Equations of high frequency vibrations of thermopiezoelectric crystal plates. International Journal of Solids and Structures 10(6), 625–637.

Moulson, A., Herbert, J., 2003. Electroceramics: materials, properties, applications. John Wiley & Sons.

Nowacki, W., 1986. Thermoelasticity. Second ed. Pergamon Press, Oxford.

Okazaki, Y., 1990. A micro-positioning tool post using a piezoelectric actuator for diamond turning machines. Precision Engineering 12 (3), 151–156.

Peacock, A., 2000. Handbook of polyethylene: structures: properties, and applications. CRC Press.

Peerlings, R., Fleck, N., 2004. Computational evaluation of strain gradient elasticity constants. International Journal for Multiscale Computational Engineering 2(4).

Saadon, S., Sidek, O., 2011. A review of vibration-based mems piezoelectric energy harvesters. Energy Conversion and Management 52 (1), 500–504.

Sixto-Camacho, L. M., Bravo-Castillero, J., Brenner, R., Guinovart-Díaz, R., Mechkour, H., Rodríguez-Ramos, R., Sabina, F. J., 2013. Asymptotic homogenization of periodic thermo-magneto-electro-elastic heterogeneous media. Computers & Mathematics with Applications 66 (10), 2056–2074.

Smits, J. G., Choi, W.-s., 1991. The constituent equations of piezoelectric heterogeneous bimorphs. IEEE transactions on ultrasonics, ferroelectrics, and frequency control 38 (3), 256–270.

Smits, J. G., Dalke, S. I., Cooney, T. K., 1991. The constituent equations of piezoelectric bimorphs. Sensors and Actuators A: Physical 28 (1), 41–61.

Smyshlyaev, V., 2009. Propagation and localization of elastic waves in highly anisotropic periodic composites via two-scale homogenization. Mechanics of Materials R59, 434–447.

Smyshlyaev, V., Cherednichenko, K., 2000. On rigorous derivation of strain gradient effects in the overall behaviour of periodic heterogeneous media. Journal of the Mechanics and Physics of Solids 48(6), 1325–1357.

Steel, M., Harrison, F., Harper, P., 1978. The piezoelectric bimorph: An experimental and theoretical study of its quasistatic response. Journal of Physics D: Applied Physics 11 (6), 979.

Trovalusci, P., De Bellis, M. L., Masiani, R., 2017. A multiscale description of particle composites: From lattice microstructures to micropolar continua. Composites Part B: Engineering 128, 164–173.

Umemiya, S., Hida, M., Aoki, T., Kondo, M., 2006. Piezoelectric properties of pzt film prepared by chemical solution deposition method. In 2006 15th ieee international symposium on the applications of ferroelectrics, 318–321.

Wang, Q.-M., Cross, L. E., 1999. Constitutive equations of symmetrical triple layer piezoelectric benders. IEEE transactions on ultrasonics, ferroelectrics, and frequency control 46 (6), 1343–1351.

Wang, Q. M., Du, X. H., Xu, B., Cross, L. E., 1999. Electromechanical coupling and output efficiency of piezoelectric bending actuators. IEEE transactions on ultrasonics, ferroelectrics, and frequency control 46 (3), 638–646.

Yan, Z., Zaman, M., Jiang, L., 2011. Thermo-electro-mechanical analysis of a curved functionally graded piezoelectric actuator with sandwich structure. Materials 4 (12), 2151–2170.

Yang, J., 2004. An introduction to the theory of piezoelectricity. Springer Science and Business Media Vol. 9.

A Tensorial notation for constitutive tensors

Constitutive equations (3a)-(3c) for a linear thermo-piezoelectric medium read

$$\begin{aligned}
&\sigma_{ij} = C^m_{ijkl}\, u_{k,l} + e^m_{ijk}\, \phi_{,k} - \alpha^m_{ij}\, \theta,\\
&D_{i=} e^m_{kli}\, u_{k,l} - \beta^m_{il}\, \phi_{,l} + \gamma^m_i\, \theta,\\
&q_i = -K^m_{ij}\, \theta_{,j},
\end{aligned} \tag{51}$$

Constitutive equations (51) can be written in a tensorial fashion (Mehrabadi and Cowin, 1990) as

$$\begin{pmatrix} \sigma_{11}\\ \sigma_{22}\\ \sigma_{33}\\ \sqrt{2}\,\sigma_{23}\\ \sqrt{2}\,\sigma_{13}\\ \sqrt{2}\,\sigma_{12} \end{pmatrix} = \begin{pmatrix} C^m_{1111} & C^m_{1122} & C^m_{1133} & \sqrt{2}\,C^m_{1123} & \sqrt{2}\,C^m_{1113} & \sqrt{2}\,C^m_{1112}\\ C^m_{2211} & C^m_{2222} & C^m_{2233} & \sqrt{2}\,C^m_{2223} & \sqrt{2}\,C^m_{2213} & \sqrt{2}\,C^m_{2212}\\ C^m_{3311} & C^m_{3322} & C^m_{3333} & \sqrt{2}\,C^m_{3323} & \sqrt{2}\,C^m_{3313} & \sqrt{2}\,C^m_{3312}\\ \sqrt{2}\,C^m_{2311} & \sqrt{2}\,C^m_{2322} & \sqrt{2}\,C^m_{2333} & 2\,C^m_{2323} & 2\,C^m_{2313} & 2\,C^m_{2312}\\ \sqrt{2}\,C^m_{1311} & \sqrt{2}\,C^m_{1322} & \sqrt{2}\,C^m_{1333} & 2\,C^m_{1323} & 2\,C^m_{1313} & 2\,C^m_{1312}\\ \sqrt{2}\,C^m_{1211} & \sqrt{2}\,C^m_{1222} & \sqrt{2}\,C^m_{1233} & 2\,C^m_{1223} & 2\,C^m_{1213} & 2\,C^m_{1212} \end{pmatrix} \begin{pmatrix} u_{1,1}\\ u_{2,2}\\ u_{3,3}\\ \frac{\sqrt{2}}{2}\,(u_{2,3}+u_{3,2})\\ \frac{\sqrt{2}}{2}\,(u_{1,3}+u_{3,1})\\ \frac{\sqrt{2}}{2}\,(u_{1,2}+u_{2,1}) \end{pmatrix} +$$

$$+ \begin{pmatrix} e^m_{111} & e^m_{112} & e^m_{113}\\ e^m_{221} & e^m_{222} & e^m_{223}\\ e^m_{331} & e^m_{332} & e^m_{333}\\ \sqrt{2}\,e^m_{231} & \sqrt{2}\,e^m_{232} & \sqrt{2}\,e^m_{233}\\ \sqrt{2}\,e^m_{131} & \sqrt{2}\,e^m_{132} & \sqrt{2}\,e^m_{133}\\ \sqrt{2}\,e^m_{121} & \sqrt{2}\,e^m_{122} & \sqrt{2}\,e^m_{123} \end{pmatrix} \begin{pmatrix} \phi_{,1}\\ \phi_{,2}\\ \phi_{,3} \end{pmatrix} - \begin{pmatrix} \alpha^m_{11}\\ \alpha^m_{22}\\ \alpha^m_{33}\\ \sqrt{2}\,\alpha^m_{23}\\ \sqrt{2}\,\alpha^m_{13}\\ \sqrt{2}\,\alpha^m_{12} \end{pmatrix} \theta,$$

$$
\begin{pmatrix} D_1 \\ D_2 \\ D_3 \end{pmatrix} = \begin{pmatrix} e^m_{111} & e^m_{221} & e^m_{331} & \sqrt{2}\, e^m_{231} & \sqrt{2}\, e^m_{131} & \sqrt{2}\, e^m_{121} \\ e^m_{112} & e^m_{222} & e^m_{332} & \sqrt{2}\, e^m_{232} & \sqrt{2}\, e^m_{132} & \sqrt{2}\, e^m_{122} \\ e^m_{113} & e^m_{223} & e^m_{333} & \sqrt{2}\, e^m_{233} & \sqrt{2}\, e^m_{133} & \sqrt{2}\, e^m_{123} \end{pmatrix} \begin{pmatrix} u_{1,1} \\ u_{2,2} \\ u_{3,3} \\ \frac{\sqrt{2}}{2}\,(u_{2,3} + u_{3,2}) \\ \frac{\sqrt{2}}{2}\,(u_{1,3} + u_{3,1}) \\ \frac{\sqrt{2}}{2}\,(u_{1,2} + u_{2,1}) \end{pmatrix} +
$$

$$
- \begin{pmatrix} \beta^m_{11} & \beta^m_{12} & \beta^m_{13} \\ \beta^m_{21} & \beta^m_{22} & \beta^m_{23} \\ \beta^m_{31} & \beta^m_{32} & \beta^m_{33} \end{pmatrix} \begin{pmatrix} \phi_{,1} \\ \phi_{,2} \\ \phi_{,3} \end{pmatrix} + \begin{pmatrix} \gamma^m_1 \\ \gamma^m_2 \\ \gamma^m_3 \end{pmatrix} \theta,
$$

$$
\begin{pmatrix} q_1 \\ q_2 \\ q_3 \end{pmatrix} = - \begin{pmatrix} K^m_{11} & K^m_{12} & K^m_{13} \\ K^m_{21} & K^m_{22} & K^m_{23} \\ K^m_{31} & K^m_{32} & K^m_{33} \end{pmatrix} \begin{pmatrix} \theta_{,1} \\ \theta_{,2} \\ \theta_{,3} \end{pmatrix}. \tag{52}
$$